University of Alberta

Design of a Permanent Magnet Synchronous Machine for a Flywheel Energy Storage System within a Hybrid Electric Vehicle

by

Ming Jiang

A thesis submitted to the Faculty of Graduate Studies and Research
in partial fulfillment of the requirements for the degree of

Master of Science

in

Power Engineering and Power Electronics

Electrical and Computer Engineering

Spring 2011

Edmonton, Alberta

Examining Committee

Dr. Andy Knight, Electrical and Computer Engineering

Dr. John Salmon, Electrical and Computer Engineering

Dr. Pierre Mertiny, Mechanical Engineering

Abstract

As an energy storage device, the flywheel has significant advantages over conventional chemical batteries, including higher energy density, higher efficiency, longer life time, and less pollution to the environment. An effective flywheel system can be attributed to its good motor/ generator (M/G) design. This thesis describes the research work on the design of a permanent magnet synchronous machine (PMSM) as an M/G suitable for integration in a flywheel energy storage system within a large hybrid electric vehicle (HEV). The operating requirements of the application include wide power and speed ranges combined with high total system efficiency. Along with presenting the design, essential issues related to PMSM design including cogging torque, iron losses and total harmonic distortion (THD) are investigated. An iterative approach combining lumped parameter analysis with 2D Finite Element Analysis (FEA) was used, and the final design is presented showing excellent performance.

Acknowledgments

I would like to acknowledge the invaluable guidance and encouragement received from my graduate study advisor Dr. Andy Knight for the research work done in this thesis. I would also like to thank my group members for their suggestions and help.

I am greatly thankful to Dr. John Salmon and Dr. Pierre Mertiny for being readers of my thesis and also being committee members to my exam.

Thanks are also due to the technical and administrative staff from the Department of Electrical and Computer Engineering, University of Alberta.

I would like to give my special appreciation to my wife Ning Guo and my parents for being constantly supportive to my studies.

Contents

List of Figures

List of Tables

List of Symbols

A	Section area
$\bar{B}$	Specific magnetic loading
$\hat{B}_c$	Peak value of magnetic flux density at back core
$\hat{B}_t$	Peak value of magnetic flux density at stator tooth
B_r	Magnet remanence
$\vec{B}_r$	Vector comprised rotor magnetic flux density
B_{rms}	Fundamental rms magnetic flux density
$\vec{B}_s$	Vector comprised stator magnetic flux density
B	Magnetic flux density
d	Mean air gap diameter
$\hat{F}$	Peak value of a rectangular-shaped mmf function
$\vec{F}$	Vector comprised force
f_{abc}	a,b,c coordinate system
f_e	Electrical supply frequency
F_n	The nth mmf harmonic function
f_{qdo}	q,d,o coordinate system
f	Electrical frequency
$\hat{H}_{airgap}$	Peak value of magnetic field intensity at air gap
$\hat{H}_c$	Peak value of magnetic field intensity at back core
$\hat{H}_{mag}$	Peak value of magnetic field intensity at magnet
$\hat{H}_t$	Peak value of magnetic field intensity at stator tooth
H_c	Magnet coercive force
$\vec{H}$	Vector comprised magnetic field intensity
i_d	Direct (d) axis current
i_{ph}	rms rated phase current
i_q	quadrature (q) axis current
I	identity matrix
$\bar{J}$	Specific electric loading
J	Mass moment of inertia

k_d	Distribution factor
k_{dn}	Distribution factor for the nth order of the harmonic
k_p	Pitch factor
k_{pn}	Pitch factor for the nth order of the harmonic
k_{w1}	Fundamental winding factor
K	Park's transfer function
l_{airgap}	Length of air gap
l_c	Length of magnetic flux path at stator back core
L_d	Direct (d) axis inductance
l_{mag}	Magnet thickness
L_q	Quadrature (q) axis inductance
l_t	Length of magnetic flux path at stator teeth
L	Inductance
l	Length
mmf	Magnetomotive force
N_{ph}	Number of turns per phase
n_s	Synchronous speed in rpm
p_e	Eddy current loss
p_h	Hysteresis loss
p	The number of machine poles
P	Permeance
P	Power
$\vec{r}$	Vector comprised length
R_g	Air gap reluctance
R	Reluctance
R	Electrical resistance
S	Apparent Power
V_{ph}	rms rated phase voltage
w_s	Slot width
w_t	Stator tooth width
W	System energy
α	Angle between rotor and stator magnetic flux density in radian

α	Electrical angle in radians spanned by a single phase belt
η	Efficiency
θ_0	Electrical initial angle between d-axis and the direction of magnetic flux generated by phase A of the armature winding currents when the motor starts
θ	Angle in radian
λ_d	Direct (d) axis magnetic flux linkage
λ_{pm}	Magnet magnetic flux linkage
λ_q	Quadrature (q) axis magnetic flux linkage
λ	Magnetic flux linkage
μ	Permeability
ξ	Rotor saliency ratio
ρ	Electrical resistivity
$\vec{\tau}$	Vector comprised torque
τ_{cog}	Cogging torque
ϕ_{av}	Average magnetic flux
ϕ_g	Air gap magnetic flux
ϕ	Magnetic flux
ω_e	Electrical speed in radians per second
ω_m	Mechanical speed in radians per second
ω_r	Electrical reference rotating speed in radians per second
ω_s	Synchronous speed in radians per second
ω	Angular speed in radians per second

List of Abbreviations

DTC	Direct torque control
EMI	Electromagnetic interference
FEA	Finite element analysis
FESS	Flywheel energy storage system
FOC	Field oriented control
He	Helium
HEV	Hybrid electric vehicle
ICE	Internal combustion engine
IPM	Interior magnets
ISS	International space station
M/G	Motor/Generator
NdFeB	Neodymium iron boron
NiH2	Nickel hydrogen
PM	Permanent magnet
PMSM	Permanent magnet synchronous machine
PWM	Pulse width modulation
rpm	Rotation per minute
SF6	Sulfur-hexafluoride
SIPM	Surface inset magnets
SmCo	Samarium cobalt
SMT	Surface mounted
SPM	Surface mounted magnets
SVPWM	Space vector pulse width modulation
THD	Total harmonic distortion

List of Subscripts

c	Back core
e	Eddy current
g	Air gap
h	Hysteresis
m	Magnetic
mag	Magnet
ph	Per phase
t	Stator tooth

Chapter 1

Introduction

1.1 Background Information

The foundations of electric machines are A. M. Ampere's discovery of the dynamic action between current-carrying conductors and Michael Faraday's principles of electromagnetic induction. Since then, electric machine design technology has undergone more than ten decades of development. Today's industrial work in the electrical field all involve primary applications of driving of various kinds of electrical machineries. With the existence of advanced technologies in fields of power electronics, optoelectronic devices, permanent magnet materials (rare earth magnets), manufacturing techniques, Hall Effect, and solid state controllers, electric machines with different operating principles and characteristics can be designed and manufactured to meet particular requirements from all kinds of applications.

In recent years, renewable and clean energies are in high demand, and are due to the constraints on the fuel resources, increasing environmental pollution, and subsequent global warming issues arising from the fuel usages. This is especially true in the automobile industry, where the usage of fossil fuels is dominating. Today, with the existence of advanced technologies, electrical energy can be applied to those industrial fields where fossil fuels were once regarded as non-replaceable. In recent years, increasing attention has been given to the design of electric machine for applications in fields where fossil fuels are normally predominant, like the automobile industry. Energy generated by the electric machine is clean and renewable, and has been considered as one of the most promising substitutes for fossil fuels.

One of the most effective solutions is the development of technologies on clean vehicle design. Successful progress in this area is marked by the commercialization of hybrid electric vehicle (HEV). Within an HEV, the traction is provided by a hybrid engine system combining two mechanisms: a fuel-driven internal combustion engine (ICE) and an electric machine. Compared to fuels energy, electrical energy can be generated with much less pollution, and it can be regenerated. The key component in the drive train of an HEV is its electrical energy storage unit. A typical storage unit for HEV applications usually includes battery packs constructed by employing lead-acid and lithium-ion technologies. However, chemical batteries have their drawbacks including toxic nature, long charging time, heavy weight and low energy density. Flywheel storage device, as an alternative battery technology has been considered and highly regarded as being suitable for a heavy HEV. Using a flywheel instead of a chemical battery to store energy can result in improvements in energy density, depth of discharge, charge-discharge cycles, and efficiency [1].

An effective energy conversion process by a flywheel battery system is mainly implemented by a well designed Motor /Generator (M/G) that is integrated within. The major requirements for flywheel M/G include the following features:

- High speed rating
- High power density
- High total efficiency
- High thermal endurance
- Low total harmonic distortion (THD) of the back emf wave form
- Low cogging torque
- Low rotor losses

This dissertation investigates the design of a permanent magnet synchronous motor/ generator (PMSM) suitable for integration in a flywheel energy storage system within a large hybrid electric vehicle (HEV). The operating requirement of the application includes wide power and speed ranges combined with high total system efficiency. Together with presenting the design process,

essential issues relating to the PMSM design, including cogging torque, rotor losses and total harmonic distortion (THD), are also discussed. Selected strategies as solutions to those issues are investigated, and results from both analytical equations and finite element analysis (FEA) simulations are compared to achieve the optimized design.

1.2 High Speed Electric Machines

In recent years, the demand for high speed rotating machines from various industrial fields has increased due to the merits of high power density and small size. Today's advanced technology in power electronics and magnetic material with low core losses has made high speed electric machines relevant to an expanding field of applications including automobiles, cogeneration systems and compressors [2]. There are many types of electric rotating machines, among which the most principal classes of rotating machines are: DC commutator machines, AC induction machines, and AC synchronous machines. There are also several other types of rotating machines that do not fit conveniently into any of these machine classes, but have special designs to meet particular requirements. Some examples of these machines include: DC homopolar machines, stepper machines and polyphase commutator machines. Figure 1. 1 below summarizes the typical classification of electric machine families.

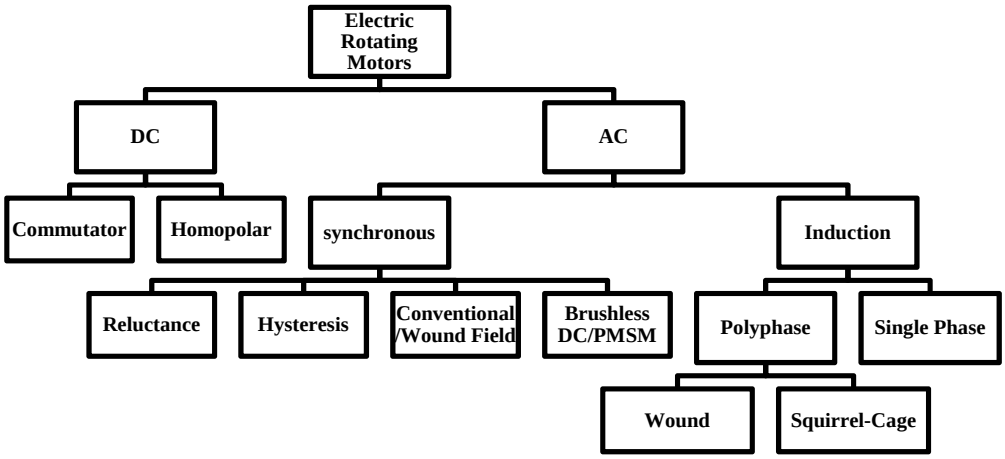

Figure 1. 1 Classifications of Electric Motors

Among the machine family members shown in the figure, the permanent magnet synchronous machine (PMSM) has become more attractive to high speed or super high speed applications. This is due to the fact that PMSM possesses many outstanding design advantages, such as relatively light weight, simple mechanical construction, high power density, and high total efficiency. Studies have also shown that the operation of PMSM involves no rotor excitation power loss and low eddy current loss in both rotor and stator, both of which result in greater total efficiency and fewer thermal side effects [3].

One example of applications requiring a high speed electric machine is the flywheel energy storage system within hybrid electric vehicles. As an energy storage device, a flywheel uses the moment of inertia of a rotating mass to store energy mechanically in the form of kinetic energy. Compared to chemical batteries, a flywheel battery possesses the following advantages [4]:

- Non-Toxic and fully recyclable
- Higher energy density and much lighter in weight
- Less charging time and deeper depth of energy discharge

- Improved power efficiency because there is no chemical reaction during energy conversion
- Temperature-insensitive operation and longer life time, the latter of which is not affected by charge/ discharge ratio
- Easier control with power electronics
- Easier and more accurate energy level measurement since the stored energy is simply related to the rotational speed
- Shortened designing time and reduced manufacturing cost

Within a typical flywheel battery, the energy conversion process is governed by an integrated electric motor/generator (M/G). As a high speed rotating device, the flywheel battery requires its M/G to have a high speed rating. As introduced before, PMSM design has great advantages for high speed applications. However, the following design issues arise due to the high rotational rates:

1. Large mechanical losses and iron losses (core losses)

Mechanical losses are mainly frictional losses due to the relative movement between surrounding air and the rotor. Iron losses are combinations of hysteresis and eddy current losses, and arise when ferromagnetic materials are excited with a time varying magnetic field. In most cases, the M/G is fully integrated with the flywheel in a vacuum enclosure to reduce aerodynamic losses and frictional losses. However, such a design also limits the ability to remove heat from the rotor, making the rotor iron losses even more difficult to be isolated. The irremovable heat may result in critical problems in the flywheel system, for example, thermal expansion of the motor composites, demagnetization, and magnetic bearing failure. Therefore, eliminating rotor iron losses becomes the most important and challenging task to the high speed PMSM design.

2. Rotor hoop stress

A high speed operating environment creates high hoop stresses resulting from the centrifugal force on both rotating wheel and rotor. Therefore, the rotating speed is limited by the tensile strength of the wheel material. If the tensile strength of a wheel material is exceeded during operation, the flywheel will shatter, and fragments can fly out with significant high kinetic energy, resulting in damages to surroundings and possible harm to people. Modern flywheel systems employ carbon-fiber composite for the rotor. Compared to steel, a carbon-fiber composite possesses advantages including lighter weight and much higher tensile strength, enabling highly improved capability of energy density and maximum operating speed. In addition to using composite material for the rotor, a securing ring surrounding the surface of rotor magnets is usually employed to protect the magnet from expansion due to the hoop stress.

The dissipation of heat in high speed electric machines presents a significant obstacle toward modern high speed electric machine design. To protect the motor from overheating demagnetization and also to obtain optimized performance, a well developed strategy for designing for high speed electric machines should be followed, including comprehensive considerations of all aspects of motor performance.

Along with studying the machine design theories and reviewing previous work, this dissertation presents a design process for a high speed permanent magnet synchronous motor which has been carried out to meet requirements for a particular flywheel battery application. In addition to the demand for high speed of rotation, the proposed electric M/G within a flywheel battery should also have high efficiency, high power density, low total harmonic distortions (THD) and low rotor losses due to the fact that the rotor is usually integrated within the vacuum enclosure.

Chapter 2

Background Theories and Literature Reviews

2.1 Flywheel Energy Storage Devices

A flywheel is an mechanical approach to energy storage. The energy is stored within a rotating device in kinetic form, and is related to the moment of inertia of the rotating mass and its angular speed as described in equation (2.1) below

$$W = \frac{1}{2} J\omega^2 \tag{2.1}$$

In equation (2.1), W is the total stored energy [Joule], ω is the magnitude of the angular velocity and J is the mass moment of inertia of the rotating device. Primary components within a typical flywheel battery are: a rotating mass, an electric Motor/Generator (M/G), a bearing system, and the control unit with power electronics. To store electricity, the flywheel is accelerated up to a desired angular velocity by the built-in electric motor, and the electrical energy used to drive the motor is converted to rotational energy. To release the stored energy, the flywheel is slowed down by the same electric machine which is now operating as a generator to provide electrical loadings. Equation (2.1) indicates that the kinetic energy stored within a rotating flywheel is proportional to the square of its angular velocity (ω^2). Therefore, if flywheels are made to be small and light yet store significant energy, they must be capable of a large angular velocity [5].

In [6] the author developed a flywheel energy storage system from first principles, and illuminated this with the $Pirouette^{TM}$ design. The author stated in the paper that the design and optimization process of a flywheel energy storage system must include considerations of the following aspects:

- Flywheel shape
- Suspension (bearing) system
- Power transfer
- Operating Losses
- Failure Management
- Manufacturability

As a promising energy storage device with multiple advantages over chemical batteries as indicated in Chapter 1, flywheel battery technology has been investigated in various fields.

In the late 1990s, a program to design, fabricate, launch, and operate a flywheel energy storage system (FESS) as means of reducing international space station (ISS) energy storage life-cycle costs was proposed by NASA Glenn Research Center (GRC). An overview of the proposed program is given in [7]. According to the manuscript, replacing the ISS's Nickel Hydrogen ($Ni\,H_2$) batteries with FESS would save approximately $500 million over the 15-year life of the ISS. The author also indicated that there are significant market opportunities and commercial potentials for flywheels validated for aerospace applications [7].

The electrical, magnetic and mechanical design data for a full scale prototype flywheel battery are presented in [8] which can be used as a reference for studying. The author illustrates a flywheel energy storage system capable of enhancing the fuel economy by being applied to hybrid electric vehicle. According to [8], a temporary energy store using a flywheel is expected to have a power density of 1kW/kg with motor efficiency of more than 90%, while conventional battery packs are capable of only 100W/kg power density with 70% efficiency. The paper also presents the prototype design process with considerations of many design variations in different aspects including material design, rotor design, magnetic design and electric design. These design procedures together with essential design parameters being discussed are common for many high speed electric machine designs.

Besides aerospace and hybrid electric vehicles, there are many other fields of studies that involve flywheel energy storage device. Examples include power distribution networks [9], electromagnetic guns [10] and micro-generator [11]. Studies on the applications of flywheel batteries are beyond the scope of this thesis, and associated contents will not be reviewed in detail.

2.2 Permanent Magnet Synchronous Machine

One key component within a flywheel system is the electric M/G, which governs the effectiveness of the energy conversion process. According to flywheel theory, the M/G in a flywheel system should be capable of a high speed rating. In addition to the demand for high speed, the electric M/G within a well designed flywheel battery should also have features of high efficiency, high power density, and low rotor losses. Many studies and research work have been dedicated to the development of PMSM for high speed applications. Based on these studies, the PMSM can provide high power density and fast response, since the use of rare earth magnet materials can increase the air gap flux density, and hence, increase the motor power density and torque-to-inertia ratio [12]. In addition, the PMSM is capable of offering the benefit of low rotor losses due to the absence of rotor windings [13]. Due to these advantages, the PMSM has been highly regarded as a suitable candidate for the M/G to be integrated within a flywheel and is chosen for the design in this thesis.

As indicated in Figure 1. 1, PMSM, also known as brushless DC machine, is an AC synchronous machine. Like all rotating electric machines, a PMSM consists of a rotor and a stator separated by a narrow air gap. Figure 2. 1 shows a top view of a PMSM structure. As indicated in the figure, the armature part for the PMSM is on the stator, and the rotor design includes permanent magnets (PM) to supply the field excitation.

A complete PMSM also consists of the bearing system and the control unit with power electronics. The operating principle behind the PMSM is similar to other AC synchronous machines: the applied current frequency in the stator windings is synchronized with the rotor rotating speed. The difference is that

within a PMSM, there are no field windings on the rotor; instead, permanent magnets are employed to supply the field excitation. With such design in place, rotor heat loss can be significantly reduced. In addition, the complication of passing field current to the moving rotor, which is a necessary step to operate conventional AC synchronous machines and induction machines with field windings, can also be avoided.

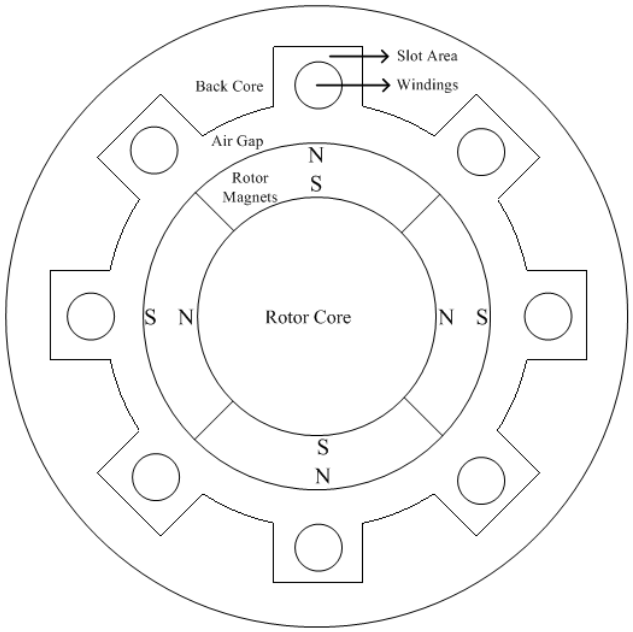

Figure 2. 1 Top View of a PMSM Structure

High efficiency is an outstanding characteristic of the PMSM. However, to achieve relatively large power levels, a PMSM requires the use of permanent magnets (PM) of types that are currently costly [14]. Permanent magnets which are made of cobalt-platinum and the cobalt-rare earth alloys, for example, are normally expensive products. Typically, rare earth neodymium iron boron (NdFeB) magnets are used for PM motor fabrication. Besides its high cost due to the high-performance permanent magnets, some other drawbacks of a PMSM include:

- Less capability of field weakening
- Operating dependence on load conditions and temperature

2.3 Origins of Energy Losses for PMSM

For the flywheel device to obtain high energy density, it is essential for its electric M/G to operate at speeds in excess of 30,000 rpm [8]. However, such high speed operations may cause windage losses, iron losses and inverter switching losses to be excessive.

As introduced in chapter 1, excessive rotor losses will result in low total efficiency and severe damage to the system. One unique and the most attractive feature of a PMSM is that almost no heat is generated inside the PM rotor because of the absence of rotor windings, which is essential to minimize rotor losses while working within a vacuum environment [13]. Ideally, the PMSM can be considered to have negligible rotor losses since the rotor rotates in synchronism with the fundamental air gap magnetic field. In practice, however, the presence of any non-synchronously rotating harmonic field induces rotor losses in both the permanent magnets and the rotor back-iron (core) [15]. Although the rotor core losses are relatively small compared to the stator losses, because of the limited ability for heat removal, the rotor core losses can cause severe damage to the machine including thermal expansion to the rotor composites and permanent magnet demagnetization. Therefore, minimizing rotor losses has become the most important and challenging task for high speed PMSM design.

Specifically, rotor losses in a PMSM are caused by some combination of the following phenomena [16]:

- Air gap permeance variation due to stator slotting
- Spatial harmonics due to non-sinusoidal winding distributions
- Time harmonics in the stator current waveform
- Eddy-current losses in rotor magnets of the PMSM induced by the tooth ripple flux contributed by stator slotting

For a complete PMSM drive system, these mechanisms of energy losses are from the power electronic inverter, the electric M/G and the bearing system. Although only the electric M/G design is the primary topic of this project, the

design cannot be implemented without considering ratings and limitations from both motor drive and bearing system. These components have considerable impact on the overall performance of the machine in practice. Therefore, issues related to drive and bearing designs should also be considered when designing a PMSM. A brief review of the potential origins of machine energy losses is given in 2.3.1 and 2.3.2.

2.3.1 Origins of Power Electronic Drive Losses

As mentioned above, the PMSM design will not go well without considering the power electronic drive. This is not only because the drive brings rating constrains to the design, but also because it is the source of one significant portion of power losses. Generally, the main performance of the drive is influenced by the pulse-width modulation (PWM) technique, the switching and conduction losses, output ripple current, and DC link current ripple [17]-[18].

The conduction losses from the drive are simply produced by the conduction of power electronics such like insulated gate bipolar transistor (IGBT) and diode. It depends directly on the modulation function that is used [17]. Some popular modern PWM schemes include Sinusoidal PWM (SPWM) and Space Vector PWM (SVPWM).

The switching losses come from the operation of IGBTs, and mainly depend on the DC link voltage, instantaneous line current, and turn on/off transition time [17]. For the PMSM design which is described in this thesis, operation at maximum switching frequency of 15 KHz will result in an increase to the switching losses. However, because of the high fundamental frequency required for the machine, it is desirable to operate the switches with a switching frequency as high as possible [19]. Therefore, limiting the root-mean-square (rms) winding current becomes even more important since it has an impact on balancing the switching losses from the drive.

There are other factors that are related to the drive operation that will result in drive losses. Two of those factors are:

- When controlling with PWM schemes, the drive will introduce a high frequency current ripple band onto the q-d axis current components, and "peak-peak excursion dictated by the switching scheme and bandwidth of the current control loop [20]", which in turn causes the distortion to the magnet magnetic flux waveform
- During the analysis, the stator magnetomotive force (mmf) distribution is assumed to be sinusoidal, but in practice, the mmf distribution is more like a trapezoidal shape due to the stator winding distribution

Like most primary AC synchronous motors, the PMSM described in this thesis is designed to induce sinusoidal back emf, and will be driven by a sinusoidal shaped voltage or current. The induced back emf waveform will contain higher frequency harmonics, which contribute to the total harmonic distortion (THD). For simplicity, some AC synchronous motor drives are designed to accept square and trapezoidal shaped voltage waveforms, which are commonly referred to as brushless DC drives. According to [20], in drives other than sine-wave driven, the rotor loss generation can become more pronounced due to the inherent motion which occurs between the rotor and stator fields.

2.3.2 Origins of Electric M/G Losses

The main contribution to the energy effectiveness of the flywheel energy storage system is from the electric M/G design. The operation of the electric machine involves energy conversion between mechanical and electrical states, and power is dissipated in various forms during the process. Figure 2. 2 illustrates the diagram of power flow in the PMSM while it is running in steady state.

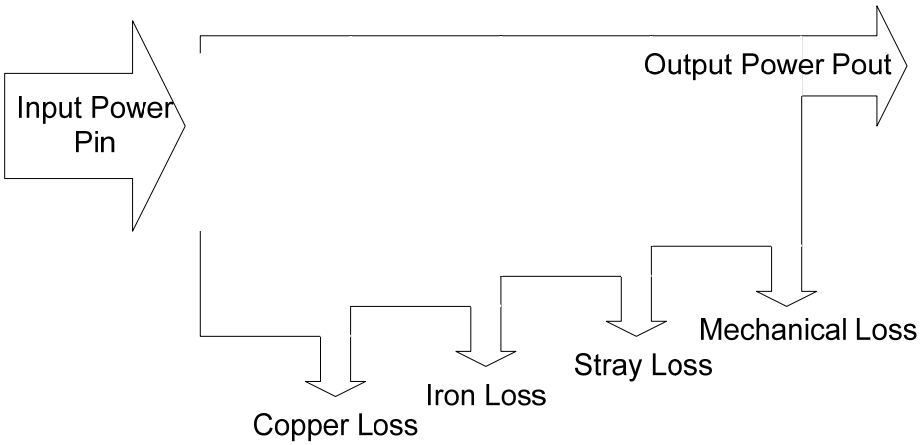

Figure 2. 2 Power Dissipations in PMSM

As indicated in Figure 2. 2, the losses of a PMSM can be decomposed into four components, namely stator winding loss (copper loss), iron loss, mechanical loss and stray load loss. In this section, brief discussions of each type of losses indicated in Figure 2. 2 are presented.

2.3.2.1 Copper I^2R Losses

The copper I^2R loss is simply the heat loss due to the stator winding resistance. The copper I^2R loss will never be totally eliminated as long as there is current flowing. However, it can be limited to an acceptable value by reducing either the rms current or the winding resistance; of course, the best strategy is to reduce both factors.

The resistance of a conductor is calculated as

$$R = \frac{\rho l}{A} \tag{2.2}$$

where R is the total resistance of the conductor, l and A are its total length and cross section area, respectively, and ρ is the resistivity. The most widely used conductor material is copper, which has a $\rho = 1.72 \times 10^{-8}$ Ωm. The length of the conductor for a single phase is mainly determined by the stack length of the motor with the consideration of allowances of the end-turn lengths. The part of the winding that is outside of the stator is called the end winding. A short-pitch winding is usually used to reduce the end winding length, resulting in reduced

copper loss [21]. While performing the analysis, the resistance is usually assumed to be constant, but in practice, the conductor resistance will increase with operating temperature.

2.3.2.2 Iron Losses

To achieve high efficiency of a high speed PMSM, the influence of iron losses cannot be neglected as they increase with the driving frequency. Based on [22], iron losses of PM machines form the larger portion of the total losses than that in induction machines. In addition, iron losses are very difficult to isolate, especially for the flywheel application where the ability to remove heat from the rotor is limited. Therefore, iron losses prediction and elimination of PM machines remain one of the most interesting and challenging topics of PM motor design [22] [23].

The iron losses are composed of hysteresis losses and eddy current losses, and arise when ferromagnetic materials are excited with a time-varying magnetic field. The typical magnetization characteristics of a ferromagnetic material can be described graphically as hysteresis loops (B-H curve) shown in Figure 2. 3

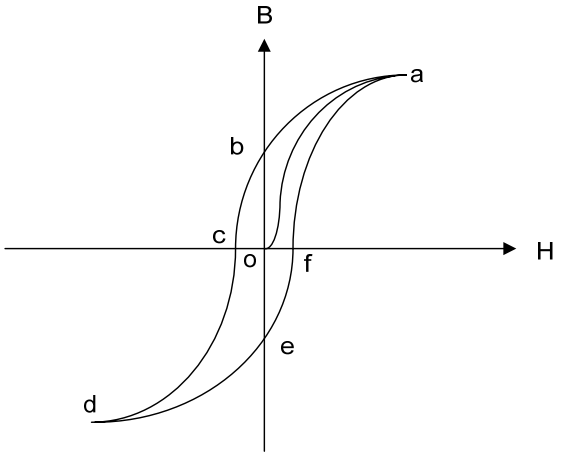

Figure 2. 3 Magnetization Characteristics of Ferromagnetic Materials

As shown in the figure, curve o-a is the original path for the magnetization of the magnetic material first excited by a magnetic field. Beginning from point a, if the magnetic field decreases back to zero, and even negative values, the B-H curve

will recoil following a new path a-b-c-d. When the magnetic field starts to increase again, the B-H curve will travel back along the third path d-e-f-a, thus a complete loop has been traversed.

Each hysteresis loop may follow a different path, but energy will be dissipated for each traverse. Hysteresis loss is proportional to the size of the hysteresis loop, and is mathematically proportional to the product of supplied frequency and the peak magnetic field exciting the ferromagnetic material [24]. Equation (2.3) shows the calculation of hysteresis loss.

$$P_h = k_h f B_m^n \tag{2.3}$$

In equation (2.3), the subscript h denotes the term of hysteresis, k_h is a constant determined by the magnetic material type and dimensions [16], B_m is the maximum flux density exciting the material, n is an exponent factor between 1.5 and 2.5 which is determined by the material [24].

Ferromagnetic materials can conduct magnetic flux very efficiently. However, they also have large electrical conductivity. Electric currents will be induced within the ferromagnetic material due to the time-varying magnetic field, and will circulate within the material causing iron losses. This circulating current is known as eddy current. The mathematical equation is also given in [24] as

$$P_e = k_e f^2 B_m^2 \tag{2.4}$$

In equation (2.4), the subscript e denotes the term of eddy current. It can be observed that eddy current loss is proportional to the square of both supply frequency and the peak magnetic field. This indicates that for operations with high supplying frequency such as the PMSM described in this thesis, the iron losses will be dominated by eddy current losses.

Iron losses can exist in the rotor core, stator core and magnets. Theoretically, the rotor of a PMSM should experience no iron losses since it always rotates in synchronism with the fundamental stator mmf, which means no time-varying excitation occurs within the rotor. However, due to slotted design, non-sinusoidal stator mmf distribution and phase current wave forms, temporal

and spatial harmonics will exist in the air gap flux field which will induce the eddy current losses in both rotor core and magnets [25] [26].

The voltage time harmonics are created by the three-phase inverter driving the motor. The switching harmonics would appear in the frequency spectrum grouped around multiples of the switching frequency (carrier), and will extend to infinity. The voltage time harmonics of the phase voltage will in turn produce current time harmonics in the stator windings, and these current time harmonics will generate spatial travelling magnetic fields that do not rotate synchronously with the rotor flux. This is mechanism by which temporal harmonics from the inverter induce rotor losses to the M/G.

Spatial harmonics arise due to the non-sinusoidal winding distributions. In practice, most armature windings of PM motors are uniformly distributed. At any time instant, the three-phase winding current can generate a three phase spatial current distribution as a function of the stator angle. Fourier series analysis can be applied to this uniformly distributed spatial current [27], resulting in equations describing traveling wave stator currents in terms of spatial sources that have a relative rotor frequency for non sinusoidal distributed windings (Refer to [28] for detailed calculations and equations). These travelling wave currents will generate air gap magnetic flux which is not synchronous with the rotor flux, and will ultimately create rotor eddy current losses.

2.3.2.3 Mechanical Losses

Mechanical loss of the motor is usually regarded as windage loss. The definition of windage loss simply is: “the loss due to the friction when there is a relative movement between air and the object”. In the case of PMSM, the object is the outer surface of the rotating rotor. In [29] a strategy of mixing He (helium) and SF6 (sulfur-hexafluoride) gas for reducing the windage loss is proposed, but the most commonly used method is to create a vacuum environment surrounding the rotor by using vacuum pump. In this case, great effort should be made to the system structure design and maintenance to avoid air leakage.

2.3.2.4 Stray Load Losses

The nature of stray loss is complex. It is actually an unexpected factor of losses over those widely acknowledged conventional losses including copper, iron and mechanical losses. This so called “stray loss” at present time had not been realized by scientists until a long while after the invention of induction motors. It was determined by load testing, and cannot be explained by any of those conventional losses. It cannot be ignored when determining the real efficiency of the motor because it typically attributes to a 10% to 20% factor of the total losses [30].

After realizing the significant impact on the motor performance that is brought by stray losses, researchers began to focus on this issue. Through years of studies and research, the causes of stray losses have been determined. Certain strategies for predicting, measuring and limiting stray losses have also been well developed. A more accurate mathematic model of PMSM taking account of all kinds of losses including stray losses is presented and discussed in [31]. In [32], the author presented a strategy for stray loss analysis using time-stepped finite elements.

According to some publications, causes of stray losses within a PM machine are related to pulsations of core flux, tooth flux, slot leakage flux and main leakage flux [30]. As mentioned in the previous section, the time-varying magnetic flux will induce core losses within both rotor and stator laminations, but these losses are examined based on the fact that the pattern of the air gap magnetic field is smooth and undistorted during the operation. This is obviously not true in practice because any motion between magnetic flux and the stator slots will cause distortion to the field. During the operation of PMSM, the magnetic flux linkage of the armature winding plus flux leakages are distorted by the slot openings, and hence cause flux pulsations at teeth and back core.

According to [30], stray losses increase with the width of slot openings. Therefore, to make the slot opening smaller, a tooth-tip is usually added to the slot. With the presence of tooth-tips, a more uniform air gap permeability, as a

function of angular position along the tooth surface can be obtained, and pulsation losses can be limited. Some stator designs do not even include teeth and slots, but simply ring-shaped laminations. The PMSM designed with such a stator is referred to as a slot-less PM machine. Slot-less PM machines include advantages of simplified design, no saturation of the stator iron, reduced stray losses, eliminated cogging torque and a linear current-torque relationship [33]. However, the slot-less PM machine has an increased magnetic air gap due to the slot-less structure, resulting in reduced air gap flux density and increased leakage [21]. This also means that the power density is reduced. Typical stator designs with teeth and slots have very mature concepts, and they are the most common modern designs for various applications.

Besides slot-tooth configurations, some other strategies for limiting stray losses include: using larger air gap length, stator coil pitch and applying Y-connected loadings instead of delta-connected [30].

2.4 Other PMSM Design Aspects

2.4.1 Cogging Torque

It is the moment of force, also known as torque that drives the PMSM to rotate. By definition, torque τ is the tendency of a force to rotate an object about an axis.

$$\vec{\tau} = \vec{r} \times \vec{F} \tag{2.5}$$

In equation (2.5), $\vec{\tau}$ is the torque, $\vec{F}$ is the applied force and $\vec{r}$ is the distance between the origin of the rotating axis and the origination of applied force. It is indicated that for non-zero torques, $\vec{F}$ must not be parallel to $\vec{r}$. During the operation of PMSM, the magnetic field generated by magnets applies primary force to the stator winding. A secondary force due to the alignment of poles which is the primary force in reluctance machines is an unexpected force for PMSM. The torque generated by this force is called cogging torque. The cogging torque is

perhaps the most annoying parasitic factor for the PMSM design since it raises torque ripple problems, reducing the quality of the output power [24].

The equation to calculate cogging torque is given in [24] and is

$$\tau_{cog} = -\frac{1}{2}\phi_g^2 \frac{dR_g}{d\theta} \tag{2.6}$$

where ϕ_g is the air gap flux, R_g is the air gap reluctance, and θ is the stator angle. The cogging torque has a close relation to the tooth harmonic and is affected by the teeth number under a pole pair [34]. Based on [34], the cogging torque frequency increases with the slot number, but its peak-to-peak magnitude reduces with frequency.

Skewing of the rotor is a standard cogging torque elimination procedure for induction machines [35], but is not quite applicable for the PMSM because it will lead to a very complicated rotor design with specially shaped magnets [36]. Instead of skewing the rotor, a PMSM design usually has the stator skewed, but such a design does not allow automatic winding production of the stator, and is usually limited to hand-wound prototypes [37]. The authors of [31] proposed a method of varying the inverter current by standard control based on pre-calculated compensation. Such method avoids the high-cost skewing design for the PMSM, and works well for lower speed applications, but it places a stringent requirement on the calculation speed of vector control.

Other selected strategies for reducing the cogging torque are: slot-less stator design or tooth-tips design, fractional-pitch winding design, implementing larger air gap, and skew designs on either magnets or slots.

2.4.2 Total Harmonic Distortion

Total harmonic distortion (THD) is an important measurement used to quantify the level of harmonics in voltage or current waveforms. The definition of THD is the percentage of harmonic components as compared to the fundamental. The equation for calculating THD is given in Chapter 4. For AC machine applications, it is desirable that supplied voltages and currents do not contain

harmonic components, i.e. with a THD of zero because harmonic components can cause many unexpected phenomena, such as electromagnetic interference (EMI) noise, torque ripple, mechanical vibrations and acoustic noise [38].

In practice, the harmonic components in motor windings are inevitable, and could be caused by various factors. Some causes, such as structural imperfection and inverter switching have been described previously in section 2.4. There are many studies on reducing torque ripples and THD in the PMSM. Some researchers have proposed filter designs in the supply side to reduce harmonics associated with power electronic drives. An active filter design which compensates the harmonics by injecting harmonics into the line current [39] is one such example. Some other studies have been focused on the loading side of the motor. An approach using self-tuning multiple-frequency resonant controllers to minimize the torque ripple of the surface mounted PMSM caused by back electromotive force (EMF) was proposed in [40]. The method is carried out by executing a control scheme in a DS1104 real-time control card to drive the studied PMSM through IGBT inverters. The proposed control scheme was analyzed in the Concordia reference frame. The experimental result successfully showed a significant drop on the torque ripple amplitude from 17.5% of the average torque to 5% by applying the proposed control scheme. In addition, the THD issues can also be improved by applying innovative control strategies.

2.5 Review of Previous Work of High Speed Electric Machine Design

Electric machine design is an advanced technology which has been developed since 1830's when Michael Faraday first introduced the law of induction. Over centuries, studies and developments on the electric motor design have not ceased because of its indispensability to numbers of applications. Nowadays, theories and principles for electrical machine analysis and design have been well defined, and a great number of creative design strategies for optimization have also been proposed and validated. Therefore, designers today

should possess adequate knowledge and resources to design and build an electric machine to implement particular tasks. Although there are already a large number of electric machine choices, since universal electric machines cannot meet the ever growing design requirements from various industrial fields, studies and researches on advanced design technologies for new generations of electric machines still draw considerable attention from researchers.

In general, it is not trivial to design and build an electric machine with the right motor topology to meet certain application requirements. Machine design process involves a wide range of technologies including mechanics, electrics, electromagnetic and thermodynamics. Like most engineering design tasks, there are always interactive variables and unpredictable factors that are difficult to define. In most cases, these unknown variables and factors need to be assumed at the beginning and then be updated based on analysis of the ideal initial design. The final design will eventually be implemented after a number of iterative design processes. The iterative process for the design of an electrical machine is illustrated by the diagram shown in Figure 2. 4 below.

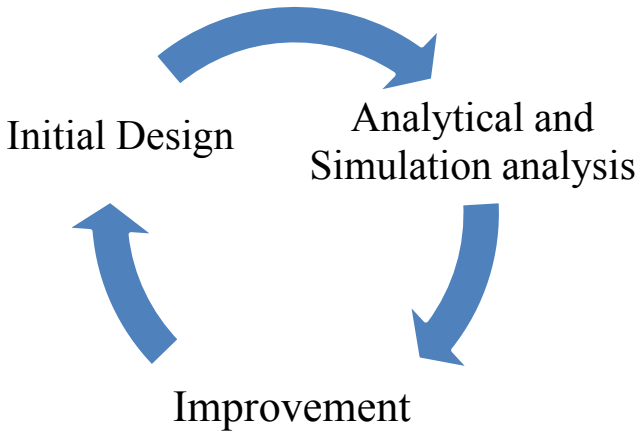

Figure 2. 4 Iterative Design Approach Visualization

As introduced in chapter 1, high speed electric machines are in high demand for today's industrial applications. The dominant factors that need to be considered for high speed electric machine design include iron losses, centrifugal forces,

fringing effects, and acoustic noise [41]. In addition, application requirements including dimensions, power ratings and speed ranges all present further constrains to the design. In this section, selected literatures regarding strategies for high speed electric machine design and previously designed work are reviewed.

The design of a high speed permanent magnet synchronous M/G for the flywheel application in a spacecraft is presented in [42]. The design consisted of the following [42]:

1. Specifications
2. Output power determination
3. Rotor topology selection
4. Main material selection
5. Main design solutions and geometry dimensions selection
6. Geometry optimization using design software
7. Finite element analysis (FEA) including transient modes
8. Final design

These machine design procedures are particularly aimed at the development of flywheel energy storage system for spacecraft applications as described in [42]. Depending on the design requirements and the emphasis of a particular application, the procedures could vary, and the sequence could also be rearranged. The listed design procedure, however, still contains the most common and essential procedures for the high speed electric motor design. Therefore, those procedures should be reviewed to provide guidelines for the design of PMSM which is the focus of this thesis.

After the specifications, the design described in reference [42] started with the determination of the rated output power demand. As introduced in the paper, the spacecraft requires its flywheel battery to maintain constant power in either charge or discharge mode during its orbit cycle, and to simultaneously apply mechanical torque for attitude control. The torque demands are illustrated by the torque curve, and the power demand is calculated by multiplying the torque by the

speed value. A constant power value of 1.3 kW is required for the energy storage during the charging mode, while a power value of 2.6 kW is required during the discharging mode. Including the power needed for attitude control, a maximum output power demand of 7.6 kW appears at the end of the discharging mode. For such a high power rating, the permanent magnet synchronous machine (PMSM) has been chosen as the type of electric M/G to be designed.

During the procedure of "rotor topology selection", three different types of rotor magnet topologies were examined: surface mounted (SMT), spoke and buried. After comparing characteristics of all three types of rotor magnet topologies under the same boundary conditions, the surface mounted magnet (SMT) was chosen due to the fact that such a rotor configuration allows for both high output power and low back EMF THD.

The main materials that will affect the motor performance are listed in [42]. The materials being considered were selected for the manufacturing of the following parts from the motor: the permanent magnets (PM), core ferromagnetic materials, magnet wires and winding insulation. According to the author of [42], choosing the right material for the PMs is very important since it determines the machine's power ratings and capability of thermal endurance. Computations and comparisons were carried out between samarium cobalt (SmCo) and neodymium iron boron (NdFeB) materials. Based on the comparisons, the NdFeB is capable of relatively higher power output. However, the SmCo has much higher temperature stability. Since the thermal issue appears more pronounced in flywheel design, SmCo was eventually chosen as the PM material. The core ferromagnetic material will have a great influence on the maximum saturation flux density and the specific core loss of the motor. As discussed in the previous section (2.3.2.2), the eddy current loss is proportional to the square of the driving frequency. Therefore, for high speed applications, the stator core loss appears to be a significant component of the total loss. In order to reduce eddy currents, laminations with smaller thicknesses are normally used for the fabrication of the stator core. In [42], high saturation cobalt iron alloy fabricated in laminations of 0.1 mm thickness were chosen for the design.

With values of electrical ratings, selected material and values of geometrical dimensions of the machine in place, a preliminary design was built using computer software. One set of preliminary design parameters are listed in Table 2. 1.

Rated power, kW	7.6
Rated voltage, V	61
Number of poles	4
Synchronous speed, rpm	50000
Outer diameter of stator, inch	5.75
Length of core, inch	0.728
Thickness of the PM, inch	0.27
Type of the PM material	SmCo
Number of stator slots	24

Table 2. 1 Parameters of the Preliminary M/ G Design from Paper [42]

The proposed design with such a parameter configuration gives a total efficiency of 98% and a THD of back EMF of 0.96%. Results were obtained from the software output.

More accurate analysis on magnetic field and PM demagnetization was carried out using the finite element method. Some strategies were applied by the author during the optimization process. Those strategies can be summarized as followings:

- Design the PMs into segments to reduce the bending stress applied by the high speed operation to the brittle SmCo material
- Using parallel magnetic field orientation instead of radial to reduce cogging torque
- Implement stator skewing to reduce high-frequency harmonics and eddy current rotor losses

The authors of [42] also pointed out that stator skewing could cause forces in the axial direction that can affect the operation of the magnetic bearing.

The design process for a PMSM prototype for a flywheel energy storage device within road vehicles is presented in [8]. The machine is capable of a peak power transfer of 25 kW, a maximum frequency of 2,500 Hz, and a total efficiency greater than 90%. Some important design topologies are highlighted in the paper.

An axial-field orientation with single rotor and double stator configuration was chosen for the motor design. As indicated in [8], a double stator configuration can help to eliminate net axial forces on the rotor of an axial field orientation machine, since the double stator will provide the return path for the magnetic flux instead of the rotor.

Neodymium-iron-boron magnets were chosen as the material for the PMs due to their superior electrical and mechanical properties compared to other magnet types. A relatively low magnetic loading for the design has been chosen in order to limit iron losses from high speed operation. An air gap winding with an air gap flux density of 0.25 T was applied in the design. With such a magnetic design in place, several advantages could be obtained [8]:

- Eliminated tooth ripple losses in the rotor
- Reduced stator iron loss due to the fact that there are no stator teeth having a high associated loss density
- Easy stator construction
- Reduced core mass
- Reduced stress concentrations in the rotor stemming from the use of thinner magnets

The number of poles of the design in [8] was set to six. This choice was determined by balancing the reduced core back depth and armature reaction fields. It is illustrated in the paper that a high pole number will result in a reduced iron loss since the core back flux density is reduced. By choosing a six-pole design,

the machine core back depth was set to 12.5 mm, resulting in a flux density of 1.06 T at the back core and a total open loop iron loss of 25 W when driven at 2500 Hz.

Investigations on design optimization for a high speed permanent magnet synchronous machine are presented in [43]. The design was intended to meet the specifications that are listed in Table 2. 2. The machine was designed to work in a high temperature environment, and the available cooling system was a water jacket. The outer diameter and the axial length are restricted by the application requirement, which presents more constrains to the design.

Continuous power rating, kW	15
Rated voltage, V	170
Number of poles	4
Operation speed, rpm	20000
Frequency, Hz	660
Rated torque, Nm	7.1
Coolant temp., °C	30

Table 2. 2 Design Specifications [43]

In order to be fault tolerant, initially the machine was designed with the following featured configurations:

- Surface mounted magnet
- Concentrated armature winding
- High machine inductance

In [43], the applied design process was illustrated with the following block diagram.

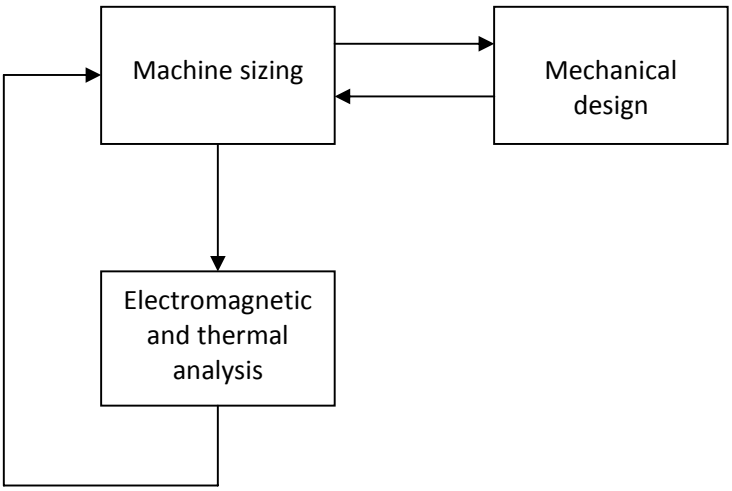

Figure 2. 5 Machine Design Methodology

Figure 2. 5 actually reflects a similar methodology to the iterative design process illustrated in Figure 2. 4. In order to obtain an optimized design, iterative analysis procedures were carried out between "machine sizing" and "mechanical design", and also between "machine sizing" and "electromagnetic and thermal analysis". The FEA method was used for rotor loss estimation and thermal analysis. Experimental results from a few design iterations are listed and compared for the determination of a certain key parameter. The key parameters that were investigated in [43] are:

- Air gap length
- Combination of magnet thickness and sleeve thickness
- Slot-pole combinations

The paper has indicated that the air gap length is a critical design parameter. It requires the designer to decide on the most appropriate distribution of losses in the rotor and in the stator [43].

Design #	1	2	3	4	5
Magnet ID (mm)	40	40	40	40	40
Magnet Thickness (mm)	6	6	6	6	6
Sleeve Thickness (mm)	2	2	2	2	2
Air-gap (mm)	**1**	**1.5**	**2**	**2.5**	**3**
hag (W/m2/K)	244	221	205	194	186
Rotor Loss (W)	464	389	357	329	306
Copper Loss (W)	199	205	220	290	330
Iron Loss (W)	210	200	194	179	173
Efficiency %	94.5	94.9	95.1	94.9	94.8
Winding Temperature °C	164	168	177	215	219
Magnet Temperature °C	255	237	231	228	223

Table 2. 3 Design Iterations : Varying The Air-Gap Length With The Highlighted Key Parameter

Based on the comparisons performed and calculated in [43], the rotor eddy current losses can be reduced by increasing the air gap length. In addition, for the same number of stator teeth and the same back iron flux density, iron losses will also be reduced with the increase of air gap length. However, for the machine to maintain the same power, the electrical loading must increase as the air gap length increases, resulting in more copper losses and higher winding temperature. Since the losses have been shifted from the rotor to the stator, the design may result in a lower total efficiency.

It has also been shown in [43] that a higher power density can be obtained by designing the machine with a distributed winding. However, if fault tolerance is a requirement, slot-pole number should carefully be selected to achieve the highest possible power density.

Chapter 3

Analysis and Design Theories

Within this chapter, operating principles and related equations for AC synchronous machine drives will be reviewed. The origins of all the equations in this section are from references [24], [44], and [58]

3.1 Basic Electromagnetic Theories

The basic laws that govern the operations of a PMSM, as well as the other electric machines are well known to be the followings:

- Current flowing in a conductor produces a magnetic field around the conductor (Ampere's Circuital law)
- The induced electromotive force (EMF) in any closed circuit is equal to the time rate of change of the magnetic flux through the circuit (Faraday's law of induction)
- The induced voltage will cause a current to flow in a closed circuit in a direction such that its magnetic effect will oppose the change that produces it (Lenz's law)
- A force is produced if a conductor conveying current is placed in a magnetic field which is non-parallel to the direction of current flow

By definition, magnetic flux ϕ is the total number of magnetic lines of force in a magnetic field. Like current in an electric circuit, magnetic flux must always form closed loops. Also, similar to the fact that electric current cannot exist without electromotive force (emf/Voltage), magnetic flux can exist only if there is a magnetomotive force (mmf). In the context of M/Gs, there are two common sources of mmf, one is from the current carrying conductor, and the other is from the permanent magnet (PM). The mmf can be calculated by Ampere's law, which states that the integral over magnetic field intensity about

any closed path in a media is equal to the total current enclosed by that path. The mathematical expression is

$$F = \oint_c \vec{H} \cdot d\vec{l} = \begin{cases} I & (if\ path\ c\ encloses\ I) \\ 0 & (if\ path\ c\ does\ not\ enclose\ I) \end{cases} \quad (3.\ 1)$$

In equation (3.1), F represents mmf, $\vec{H}$ is the magnetic field intensity, I is the total current enclosed by the magnetic flux path, and $\vec{l}$ is the total length of the path. A single loop of conductor is called a turn, and a winding of N turns forms a coil. Figure 3. 1 shows an N-turn coil winding around a magnetic core to form a simple magnetic circuit.

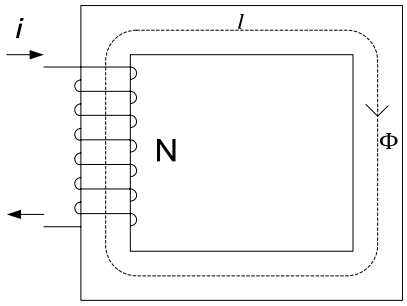

Figure 3. 1 A Magnetic Circuit

In Figure 3. 1, ϕ is the magnetic flux which can be considered as analogous to the current from the electrical circuit; i is the current driven into the coil, and l represents the magnitude of the total length of magnetic flux path. The reluctance R is defined as

$$R = \frac{1}{P} = \frac{l}{\mu A} \quad (3.\ 2)$$

where P is called permeance, which is the inverse of the reluctance R, A is the cross section area of the media, μ is the permeability, indicating the media's ability to allow magnetic flux flow. As observed in the equation (3.2), R is a function of length, cross sectional area and permeability of the media, but is not affected by external forces. That is, the reluctance R is an inherent property of the media conveying magnetic flux. The reluctance within a magnetic circuit plays the same role as the electric resistance R within an electrical circuit. By

combining equation (3.2) with equation (3.1), the magnetic circuit equation may be re-written as

$$mmf = Ni = \phi R \tag{3. 3}$$

In practice, not all magnetic flux ϕ links every single turn from a coil, but for Faraday's law of induction working, only turn-linking flux will take effect. Therefore, a more convenient quantity called flux linkage is introduced, and it is obtained by summing the flux linked by each turn of a coil. The flux linkage, λ is defined as

$$\lambda = \sum_i N_i \phi_i \tag{3.4}$$

Obviously, if there is no flux leakage, (i.e. all flux links all of turns of a coil), $\lambda = N\phi$. Now, Faraday's law of induction could be expressed in a more general way (Lenz's Law)

$$e(t) = \frac{-d\lambda(t)}{d(t)} \tag{3.5}$$

where $e(t)$ is induced voltage (back emf) in the time domain (negative sign in the equation indicates that the direction has been changed).

If it is assumed that $\lambda = N\phi$, and by using equation (3.3), the flux linkage can be calculated as

$$\lambda = \frac{N^2}{R} I = LI \tag{3.6}$$

This is a more practical and effective description of the relationship between the magnetic and electric fields. The two fields are linked by the inductance L. Ideally, this relationship is linear if the saturation of magnetic material is ignored. However, in practice, this linear relationship cannot be held throughout the entire operation since there is always flux leakage existing, and all magnetic material will saturate at a certain level of magnetization. In order to obtain the accurate design, the real values of magnetic flux linkage at rated operating conditions must be determined. At present, FEA simulation analysis using computer software is one of the most useful and effective methods for accurate magnetic field analysis.

3.2 Operating Principles for PMSM

3.2.1 Motor Generator Operation

AC motors are driven by an alternating current or voltage source, usually having a sinusoidal wave form. The placement of AC motor windings differs from that of DC motors. The power winding or armature winding of an AC machine is on the stator, while the field winding is on the rotor. As an AC synchronous machine, the PMSM has the similar structure configuration except for its rotor design. Instead of field winding on the rotor, the PMSM has a rotor designed with permanent magnets to provide rotor magnetic field flux. The operating principle of a PMSM is still the same as the other AC synchronous machines, which can be summarized as: supplied frequency in the stator winding is in synchronism with the rotor rotating speed. The synchronous speed is defined as

$$\omega_s = \frac{4\pi f_e}{p} \tag{3.7}$$

$$n_s = \frac{120 f_e}{p} \tag{3.8}$$

where f_e is the electrical supply frequency in Hz, and p is the number of machine poles. The value of p is always a multiple of 2, indicating magnetic N pole and S pole respectively. The mechanical speed ω_m and electrical speed ω_e are linked by p as

$$\omega_e = \frac{p}{2}\omega_m \tag{3.9}$$

Like most the other AC synchronous machines, a PMSM can be operated as either a generator or a motor. During the generator action, the rotor is started by an external force, for example a turbine, then the rotating magnetic field from the magnet on the rotor sweeps across the stator winding with an angular speed of ω_m, causing the back EMF to be induced. During the motor action, three-phase AC currents with frequency f_e are injected into the armature winding which will in turn generate a rotating magnetic field to interact with the magnetic field from

the rotor. The above phenomena show that there are always two rotating magnetic fields chasing each other, or trying to synchronize during the operation of PMSM. When generating, the power flow is from mechanical to electrical, and the leading magnetic field is from the magnets; when motoring, the power flow is in the opposite direction, and the leading magnetic field is from the AC winding currents.

The product of torque and mechanical speed is the power.

$$P = \tau\omega_m \tag{3.10}$$

In equation (3.10), P represents the power. When analyzing PMSM performance, it is more convenient to consider torque as generated by interference between two magnetic flux densities, the one from magnets on the rotor, $\overrightarrow{B_r}$ and one from the winding on the stator, $\overrightarrow{B_s}$. The energy view of equation (3.10) is

$$\tau = \frac{dW}{d\alpha} \tag{3.11}$$

where W is the energy in Joules, and α is the angle between $\overrightarrow{B_r}$ and $\overrightarrow{B_s}$. It can be proven that with a non-salient motor design, i.e, when inductances along both direct and quadrature axis are identical, the torque can be calculated as

$$\tau = kB_r B_s \sin\alpha \tag{3.12}$$

It is indicated in equation (3.12) that the maximum torque can be produced if $\overrightarrow{\mathrm{B_r}}$ and $\overrightarrow{\mathrm{B_s}}$ are perpendicular to each other. This is the basis of the idea of "Field Orientation Control", which is discussed in the following section.

3.2.2 Field Oriented Control (Vector Control)

Although this thesis focuses on the design of an electrical motor suitable for a flywheel energy system, and the drive design are not within the primary scope of this thesis, the machine design cannot be considered in isolation.

A complete PMSM drive system usually consists of a converter with power electronics, the PMSM itself, the sensor, and a control algorithm [44]. Figure 3. 2 shows the block diagram of the PMSM drive scheme.

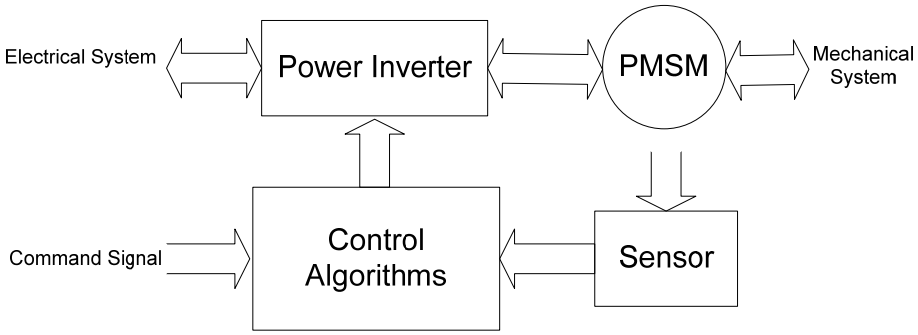

Figure 3. 2 Block Diagram of A PMSM Drive

The type of the drive is determined by the structure of the control algorithm. Analysis of the electrical machine is based on applied control strategies. For the PMSM, the most popular selected control methods are direct torque control (DTC) and field orientation control (FOC) or vector control.

DTC was introduced in the middle of the 1980s, almost simultaneously by Depenbrock and by Takahashi and Noguchi [45]. It was originally proposed for induction motor drives, and has later been applied also to synchronous machines. The basic concept behind the DTC of an AC drive is to control the electromagnetic torque and flux linkage directly and independently by the use of six or eight voltage space vectors found in lookup tables. DTC scheme provides very good dynamic responses since this method does not need PI regulators typically associated with current regulated PWM torque-controlled drives [46]. In addition, because the DTC scheme does not need the current controller, the time delay caused by the current loop is eliminated. However, there are some drawbacks of using DTC scheme:

- the variation of the switching frequency by hysteresis band and speed
- the increase of the torque ripple in the low speed region
- difficulties to accurately estimate stator flux-linkage and rotor speed

The FOC scheme which was introduced more than 25 years ago transforms the motor equations into a coordinate system that rotates in

synchronism with the rotor flux vector. Transforming the 3 phase AC motor equations into field coordinates makes the FOC method resemble the decoupled torque production in a separately excited DC motor [47] (Brushless DC machine). Referring to such a coordinate system, the rotor flux amplitude appears to be constant, and there is a linear relationship between the control variables and the torque. For the PMSM, the control variables are two field-coordinate components decomposed from the armature currents: the direct component i_d for the rotor field control and the quadrature component i_q for the torque control. Typically, the PMSM is designed such that the rotor magnet alone is capable of providing required air gap flux, that is, $i_d = 0$ up to the rated speed [48]. In this way, all supplied current from the DC link of the inverter contributes to torque production, and hence, maximum torque can be obtained. Over the years, FOC techniques have established a substantial worldwide market which continues to grow [49]. FOC was selected for the PMSM design in this thesis because it was realized that controlling currents is much more convenient, with additional benefits including optimized performance through a wide speed range and reduced torque rippling.

The regular 3 phase coordinate system f_{abc} can be transformed into a rotating coordinate system f_{qdo} through the well known Park's transfer function shown in equations (3.13) and (3.14) below [44].

$$f_{qdo} = K f_{abc} \tag{3.13}$$

$$K = \frac{2}{3}\begin{bmatrix} cos(\omega_r t) & cos(\omega_r t - \frac{2\pi}{3}) & cos(\omega_r t + \frac{2\pi}{3}) \\ sin(\omega_r t) & sin(\omega_r t - \frac{2\pi}{3}) & sin(\omega_r t + \frac{2\pi}{3}) \\ \frac{1}{2} & \frac{1}{2} & \frac{1}{2} \end{bmatrix} \tag{3.14}$$

If the rotating speed of f_{qdo} is synchronous with the supplied frequency f_e, the supplied AC current can be treated as two separated constant DC components in the new coordinate system. In equation (3.14), ω_r represents the reference rotating speed in electrical rad/s. The new coordinate system consists of a quadrature axis (q), a direct axis (d) and a common component (o), where the d-axis is aligned to the direction of rotor flux, q-axis leads d-axis by 90 electrical

degree, and the o-axis is normally cancelled out. The reference frame could be different due to the definition of ω_r, for example a stationary reference frame has a reference rotating speed $\omega_r = 0$. While performing analysis on synchronous machines, the most suitable reference frame is the rotor reference frame, where

$$\omega_r = \omega_e + \theta_o = 2\pi f_e + \theta_o \tag{3.15}$$

and θ_o is the initial angle between the d-axis and the direction of magnetic flux generated by phase A of the armature winding currents when the motor starts.

3.2.3 Analysis Equations for PMSM

As mentioned above, a PMSM employing vector control is favorable for high performance drive applications since it fulfills the design criteria of compact structure, high air gap flux density, high power to inertia ratio, high torque to inertia ratio and high torque capability [50]. The basic idea of the vector control has been introduced above, while in this section, the PMSM lumped parameter equations in the f_{qdo} rotor reference frame will be derived.

Although PMSM could be treated as either a generator or a motor, investigations will be carried out based on motoring condition only. While for the generating condition, equations could be deduced by simply inverting the operator signs. For a three phase sinusoidal supplied synchronous motor, the armature circuit equations is

$$v_{abc} = r_{abc} i_{abc} + \frac{d\lambda_{abc}}{dt} \tag{3.16}$$

where v is phase voltage, r is the resistance of the conductors, and i is phase current (if the sign of the term $r_{abc} i_{abc}$ is inverted in equation 3.16, the equation would represent a generating condition). For a balanced three phase system

$$r_{abc} = \begin{bmatrix} R & 0 & 0 \\ 0 & R & 0 \\ 0 & 0 & R \end{bmatrix} I \tag{3.17}$$

In equation (3.17), I represents the 3x3 identity matrix. By applying Park's transfer function to equation (3.16) and a few modifications, the armature

equations in f_{qdo} can be obtained. The following steps illustrate the transfer process:

$$v_{qdo} = KrK^{-1}i_{qdo} + K[\frac{d}{dt}(K^{-1}\lambda_{qdo})] \tag{3.18}$$

$$\Rightarrow \quad v_{qdo} = RIKK^{-1}i_{qdo} + K\frac{d}{dt}K^{-1}\lambda_{qdo} + KK^{-1}\frac{d}{dt}\lambda_{qdo}$$

$$\Rightarrow \quad v_{qdo} = ri_{qdo} + \omega\lambda_{dq} + \frac{d}{dt}\lambda_{qdo} \tag{3.19}$$

and finally

$$v_q = R\, i_q + \omega_r\lambda_d + \frac{d}{dt}\lambda_q \tag{3.20}$$

$$v_d = R\, i_d - \omega_r\lambda_q + \frac{d}{dt}\lambda_d \tag{3.21}$$

The torque equation for all electric machines can be derived based on an energy view of (3.11) as

$$\tau = \frac{3}{2}\frac{p}{2}\left(\lambda_d i_q - \lambda_q i_d\right) \tag{3.22}$$

where *p* represents number of machine poles. For PMSM,

$$\lambda_d = L_d i_d + \lambda_{pm} \tag{3.23}$$

$$\lambda_q = L_q i_q \tag{3.24}$$

where λ_{pm} represents magnet magnetic flux linkage. Equations (3.20) through (3.24) are well known PMSM lumped parameter equations. It is indicated in equations (3.20) through (3.24) that after transforming to a rotor reference frame f_{qdo} coordinate system, all parameters can be defined separately along two independent axis, one is along the rotor magnetic flux source (d) and the other is quadrature axis (q) which is 90° electrically leading. This will obviously simplify the analysis.

By combining equations (3.22), (3.23) and (3.24), the torque equation can be developed further:

$$\tau = \frac{3}{2}\frac{p}{2}\left[\lambda_{pm} i_q + \left(L_d - L_q\right) i_d i_q\right] \tag{3.25}$$

It can be seen from the equation that keeping $L_d = L_q$, a linear relationship between torque and current along q axis can be obtained. This is actually a scenario described by equation (3.12) for the maximum torque to be produced. Equation (3.12) indicates that a maximum torque will be obtained when there is a 90° electrical angle between rotor and stator magnetic flux density vectors. This is reflected by equation (3.25) as controlling the stator magnetic flux density along the q- axis while leaving rotor flux density along the d- axis. This also implies that there will be no stator current participating along the d- axis and all stator currents may be attribute to the torque (except for the case when injecting $-i_d$ for field weakening is required). Since the stator current can be controlled by the DC link current, a linear relationship between torque and supply DC current can be obtained. The following figure shows a simple close-loop control schematic with DC current supply for a PMSM system:

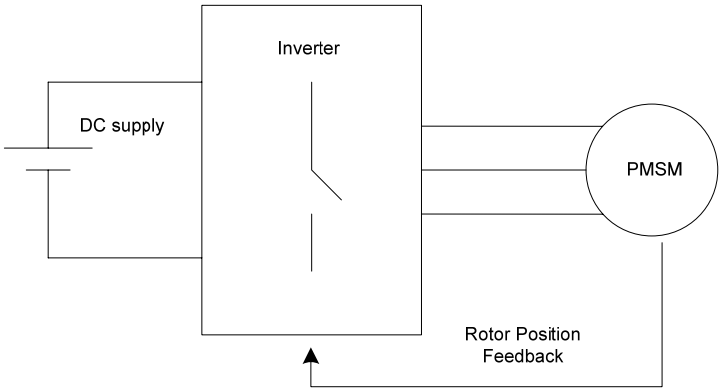

Figure 3. 3 A Closed Loop Control Schematic for PMSM

For steady state analysis, the derivative terms from both equations (3.20) and (3.21) (the last term of the right hand side of the equation) can be ignored.

3.3 Analysis and Design Principles for PMSM

3.3.1 Analysis and Design Tools

Machine analysis and design work can be viewed as two opposite processes. While performing analyses, key factors such as the machine configurations, working condition and control method are all set. The results can be obtained by directly testing the operating system, and then very straightforward analysis equations can be applied to help determine the most important parameters. Some of those key parameters that are normally used to measure a motor's performance are the total efficiency (η), the total harmonic distortion (THD), torque ripple levels, current dependence on speed and the torque to mass ratio.

While designing, only the ratings of the machine and how well the machine is expected to perform its duty are known factors. Many unknown parameters including structure dimensions, choice of materials and various other design configurations are required to be determined to reach the design goal. However, to keep the design process on the right track, machine analysis should be carried out throughout every stage of the design process.

Electric machine design is complex, and involves a number of techniques and calculations. Appropriate analysis and design tools should be applied to obtain the most accurate data, and hence, the best design. For this particular PMSM design, tools being used for analysis and design are spread sheets, Matlab, and JMAG. JMAG is a commercial electromagnetic field analysis software applying FEA. Steady state analysis based on equations is carried out with spread sheet; JMAG is used to build the 2-D model for the motor, carry out analysis on heat and magnetic field, and provide simulation results which again will become the new input parameters for both spread sheet and Matlab.

3.3.2 Parameters and First Principles

The theoretical design process for this particular PMSM design has followed similar procedures introduced in [42], which was reviewed in Chapter 2.5. Electric machine ratings and design specifications should be determined first. The power rating of an electric machine indicates the amount of power that the machine is capable of delivering for a sustained period of operating time. The factors that will directly affect the power rating of the machine include:

- The amount of heat due to the internal losses, that the machine can dissipate before the temperature rises beyond the level that the conductor insulator can tolerate
- The magnetic flux saturation level in the iron that the machine can tolerate before excessively large currents are required to magnetize the machine

The above factors are essentially related to the machine performance, and should be considered during the design process for the machine to meet its ratings.

One thing has not been introduced in [42] is the first principle that can relate machine ratings to its structural designs. In order to derive the first principle, some parameters have to be defined in advance. Essential design parameters that are related to various machine specifications including electric, magnetic and structural are listed in Table 3. 1 below.

Symbol	Description
S	Apparent power
n_s	Synchronous speed in rpm
l	Stack length
d	Mean air gap diameter
p	Number of poles
N_{ph}	Number of turns per phase
n_s	Synchronous speed in rpm
$\bar{B}$	Specific magnetic loading
$\bar{J}$	Specific electric loading
k_{w1}	Fundamental winding factor
B_{rms}	Fundamental rms magnetic flux density

Table 3. 1 List of Design Parameters

For a three-phase electric machine, the power rating can be defined by the following equation

$$S = 3V_{ph}I_{ph} \tag{3.26}$$

where V_{ph} and I_{ph} represent rms values of rated phase voltage and phase current respectively. Based on Faraday's law, the rms phase voltage or rms emf of an electric machine may be defined as

$$V_{ph} = \frac{2l\omega d}{p} N_{ph} k_{w1} B_{rms} \tag{3.27}$$

If the stator winding can be assumed to be ideal, (i.e., zero winding factors for all harmonics other than the fundamental), the magnetic flux density along the stator surface for a sinusoidal air gap field distribution can be calculated as

$$B_g = \sqrt{2}B_{rms}\cos\left(wt - \frac{p}{2}\theta_0\right) \tag{3.28}$$

where θ_0 is the initial angle. Then the average air gap magnetic flux density which is measured over one pole pitch can be calculated from equation (3.28) as

$$\bar{B} = \frac{2\sqrt{2}B_{rms}}{\pi} \tag{3.29}$$

In equation (3.29), $\bar{B}$ is called the specific magnetic loading. The rms phase current can also be replaced by a parameter that holds more physical meaning. This parameter is the specific electric loading $\bar{J}$, which represents the rms value of the linear current density wave situated on the inner stator surface:

$$\bar{J} = \frac{6N_{ph}k_{w1}}{\pi d} I_{ph} \tag{3.30}$$

By rearranging equations (3.27), (3.29) and (3.30), and substituting into equation (3.26), the new equation for power rating can be obtained

$$S = \frac{2\pi}{\sqrt{2}} \frac{\omega}{p} \frac{\pi d^2 l}{4} \bar{B}\bar{J} \tag{3.31}$$

Now, by substituting $\frac{\omega}{p} = \frac{\pi}{60} n_s$ to the above equation, the final power equation containing information of factors that will directly affect the machine performance is obtained:

$$S = \frac{\sqrt{2}\pi^2}{60} \left(\frac{\pi d^2 l}{4}\right) n_s \bar{J}\bar{B} \tag{3.32}$$

Equation (3.32) is the first principle for the design of electric machines with cylindrical shape. It has indicated that the machine rating is directly related to the physical size of the machine, the synchronous speed (rpm) and the product of the specific electric loading and magnetic loading. That is

$$S = \frac{\sqrt{2}\pi^2}{60} (Air\ gap\ volume)(Syncronous\ speed)(Products\ of\ loadings) \tag{3.33}$$

In most machine design projects, including the PMSM design described in this thesis, the power rating and speed demand are normally given as requirements. Therefore, most work has been dedicated to determining parameters for machine size and machine loadings. It is indicated in (3.33) that for a given power rating and a given speed rating, the size of the machine can only be reduced by increasing the product of permissible electric and magnetic loadings.

3.3.3 Design Parameters

As introduced in the previous section, the machine design fundamentals are derived from the first principle. The first principle which is described in equation (3.33) relates the physical dimensions of the machine, the electric loading and magnetic loading to the output power of the machine. During the real design process, the machine has to be designed in accordance to the specifications. There are many design parameters that affect the overall performance of the machine. In order to obtain an optimized high speed machine design, strategies for identifying various design parameters should be carefully studied. Several selected sensitive design parameters are introduced in this section. Furthermore, the influences that each parameter has on the machine are also investigated.

3.3.3.1 Prediction of Specific Magnetic Loading and Current Loading

As mentioned above, both specific magnetic loading and electrical loading are key factors that have formed the first principle. According to equation (3.33), a PMSM with predetermined power and speed ratings leaves only the variables of air-gap volume and the product of machines loadings. Choosing the values of machine loadings needs to follows strict set guidelines. Therefore, these variables will be chosen and the remaining air-gap volume will be dictated by equation (3.33).

For higher efficiency, a synchronous machine is normally designed to work around the knee of the magnetization characteristics of its iron material [51] (please refer to Figure 2. 3 for magnetization characteristic of a material). However, exceeding magnetic density will cause the iron to be heavily saturated, resulting in a large magnetic loading to the machine, which in turn will result in excessive iron losses. This is especially true for high speed machines. Therefore, the specific magnetic loading will define the maximum magnetic flux density that the machine can tolerate without causing excessive heat loss.

The specific electric loading ($\bar{J}$) is defined as the maximum current density that can be withstood by the machine before excessive heating occurs, and sets similar bounds as the specific magnetic loading ($\bar{B}$). As mentioned before, excessive heating can cause failure of the conductor insulation. In the case of magnetic loading, an upper limit was placed on the magnetic flux density in order to avoid large magnetic loading. The case of electric loading, however, is dealt with simply by active cooling. For smaller machines, fans are normally used to circulate air, and thus, remove heat from the system. For fairly large machines, more aggressive cooling methods can be used and include replacing the air with hydrogen and liquid cooling. Thus, a better cooling system can bring an optimized electric loading factor to the machine.

Generally, at the first step of the initial design, both specific magnetic loading and electric loading have to be predicted. In [52], the author introduced a method for the prediction of the air-gap flux density as the first design step for a PM brushless motor. The method is based on the solution of Maxwell's equations. In this analysis, iron permeability and motor length are both assumed to be infinite, and due to cylindrical symmetry, only the axial component of the magnetic vector potential exists, while only the radial and azimuthal components of flux density and magnetic field strength exist. Applied equations and detailed analysis are presented in paper [52]. One other method to estimate values for machine loading at the initial stage of the design is simply by assumption. Based on design experience from the history, typical values of magnetic loading are $\bar{B}$ = 0.2-0.8 T, and typical values of electrical loading are $\bar{J}$ = 10000-40000 A/m [51]. Adjustment should be made according to particular design specifications.

3.3.3.2 Effective Air Gap Length

It is indicated in equation (3.33) that once specific machine loadings are predicted, the air gap volume can be calculated to meet the required machine ratings. Then the air gap length is now required to set the rotor boundary. The effective air gap length is slightly different from the actual air gap length by taking into the effect of stator slotting to the air gap magnetic flux density. A

coefficient known as Carter coefficient is used to convert the actual air gap length to the effective one. Carter's coefficient express the ratio between the air gap flux density without slotting to the one with slotting, and is determined by slot width, tooth width and actual air gap length [53].

Effective air gap length is one of the most important parameters to be determined during the initial design since it plays a major role in the motor performance. A large air gap helps reduce the variation in air gap flux density due to stator slotting, which in turn reduces cogging torque and induced eddy current losses in the surface mounted magnets [19]. However, large effective air gap length does not always bring benefits to the design. With an increased effective air gap length, according to the first principle, the specific electric loading has to be increased accordingly to maintain the power rating. This will result in increased copper losses. In [43], the author illustrated the influences of varying effective air gap lengths by comparing results from multiple designs. It is indicated that effectively increasing air gap length causes machine losses that shift from the rotor to the stator [43]. Therefore, the effective air gap length has to be determined by considering the overall machine efficiency. In addition, with a large air gap in place, the magnet length has to be increased to keep the air gap flux constant. This will result in increased magnet-to-magnet leakage flux and increased cost [24]. However, the air gap length must be sufficiently large to accommodate magnets if surface mounted, and allowance must be made for any possible rotor expansion due to centrifugal forces.

3.3.3.3 Rotor Design

Based on where the magnets are placed on the rotor, the PMSM can be divided into four common types: surface mounted PMSM (SPM), surface inset PMSM (SIPM), Interior PMSM (IPM) and interior PMSM with circumferential orientation [53]. Figure 3. 4 below presents the structures of the four types of rotor designs.

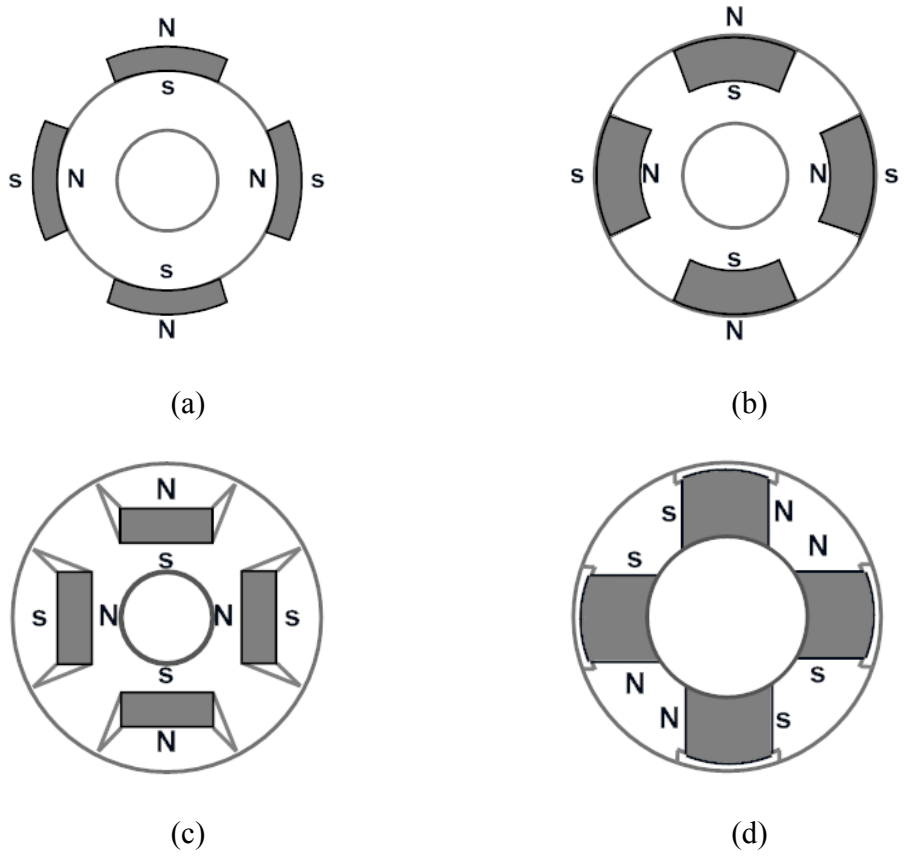

Figure 3. 4 Types of Rotor Designs Based on Magnet Placement (a) Surface mounted (SPM). (b) Surface inset (SIPM). (c) Interior (IPM). (d) Interior with circumferential orientation

Rotor permanent magnet placement has an impact on various PMSM design aspects including air gap flux density, winding inductances, reluctance torque, etc. Surface mounted PMSM is known to be able to provide the highest air gap flux density. However, such a configuration has lower structural integrity and mechanical robustness since the PMs are not snugly fitted into the rotor laminations to their entire thickness [53]. Especially for high speed applications, reinforcement to the strength of rotor structure should be applied. Kevlar tape and secure ring are often employed to the rotor design to make the rotor structure more robust.

Despite of the lower structural strength, surface mounted PMSMs possess outstanding advantages such as high power density and low back EMF [42], as well as the small reluctance variation between the direct and quadrature axes [53]. In [54], the FEM method is used to analyze and compare 3 types of rotor design

(SPM, SIPM, IPM). The results have shown that surface mounted PMSM exhibits the lowest rotor core losses and lower magnet eddy current losses. Therefore, surface mounted PM is very popular for rotor design.

Choices of permanent magnets are also very important to the PMSM design. Referring to Figure 2. 3, a PM exhibits its demagnetization characteristics in the second quadrant of the graph of its hysteresis curve, where the intensity is along the negative x-axis.

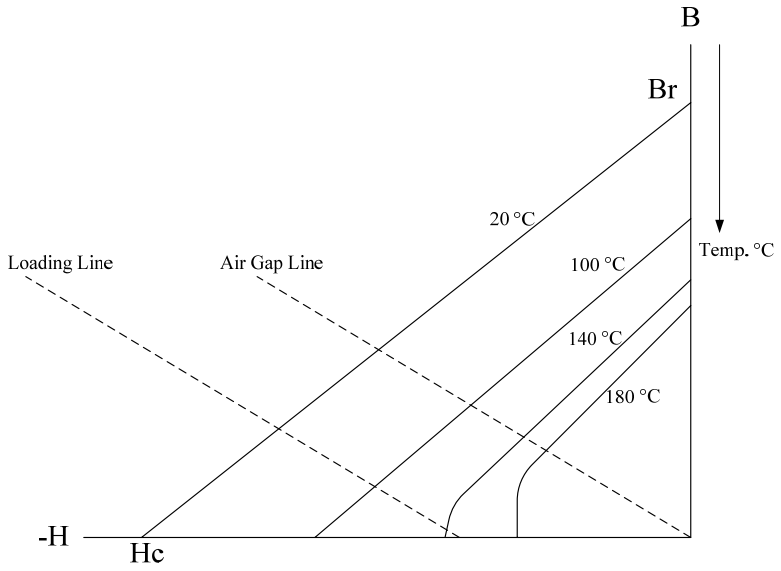

Figure 3. 5 Typical Magnetizing and Temperature Characteristics of NdFeB PM

Figure 3. 5 shows typical NdFeB permanent magnet demagnetization curves for 4 different operating temperatures. Concepts shown in the figure are:

- Residual Flux Density, or Remanence, B_r: The maximum flux density that the magnet can produce by itself; measured at the point where $H = 0$ on the B-H curve
- Coercive Force, H_c: The demagnetizing force representing the magnetic ability to induce a magnetic field when the surrounding material has zero permeability; measured at the point where $B = 0$ on the B-H curve, and usually in the unit Oersted (Oe), 1Oe=79.58 A/m

- Knee: The point on the B-H curve where the curve starts to bend, or shrink toward the origin
- Air Gap Line: The loading line where only mmf reduction, due to the air gap is considered; started from the origin
- Current Loading Line: The loading line with stator windings energized; still parallel to the air gap line but has shifted because of the demagnetization due to the stator current

It is indicated in the figure that the remanence and coercivity of an NdFeB PM decreases with temperature. The grade of deduction varies depending on the quality of the selected magnet. It is very important to ensure that the magnet will operate within the linear sections of these curves at different temperatures. During initial design, only the air-gap line requires consideration, but it should be kept in mind that under load cases, the loading line from the curve will be shifted left, resulting in much more sensitivity to the increasing temperature. Therefore, choosing stronger magnets and keeping the operating point far away from knees are always good practices for magnet design. Some common PM materials and their characteristics are listed in Table 3. 2 below.

	Residual Flux Density (Br)	**Coercivity (Hc)**	**Temperature Coefficiency**	**Cost**
AlNiCo	High	Low	Very Low	Low
Ferrites	Fairly Low	High	Fairly low	Low
SmCo	High	Very High	Low	Very High
NdFeB	High	Very High	High	Fairly High

Table 3. 2 Characteristics for Selected PM Materials

Among those materials listed above, both samarium Cobalt (SmCo) and Neodymium iron boron (NdFeB) are rare earth magnets which exhibit great capability of producing magnetic flux. Although NdFeB are strongly sensitive to temperatures, a maximum operating temperature of 170°C [56] is sufficient for

most PM machine applications. Its reduced cost makes it more economical than SmCo magnets. They also have features of high energy, ranging from 8 MGOe to 64 MGOe, great coercive force, high resistance to demagnetization, and moderate temperature stability. With these facts, NdFeB magnets have become today's preferred choice for magnets in commercial applications.

The NdFeB magnets are available in sintered and bonded forms. The sintered NdFeB magnet has a higher capability of flux production, while the bonded NdFeB magnet has a low electrical conductivity, which is good for limiting eddy currents.

In some special designs, salient rotors (as applied by reluctance machine) are employed to achieve specific torque-speed characteristics. A salient rotor is designed in such a way that the d-axis inductance, L_d, is smaller than the q-axis inductance, L_q. The ratio $\xi = \frac{L_q}{L_d}$ is called the rotor saliency ratio, and it is equal to 1 for a non-salient rotor. For some applications, low flux linkage might be designed to obtain extended operating speed range (constant power region from typical torque-speed characteristics of an electric machine). In this case, a lower torque will appear at the start (constant torque region). However, based on the results presented in [55], a higher rotor saliency ratio can be designed to restore the torque. However, the simulation results also show that this does not affect the torque to speed characteristics within the constant power region [55].

3.3.3.4 Armature (Stator) winding design

The stator of a PMSM can be either designed to have a slot-tooth structure or a slot-less structure. A slot-less PM machine only contains a ring-shape stator lamination, resulting in advantages of simplified design, no saturation of the stator iron, reduced stray losses, eliminated cogging torque and a linear current-torque relationship [33]. However, the slot-less PM machine possesses low starting torque and low total efficiency due to the high iron losses [57]. Typical stator designs with slot-tooth structures are the most popular designs for modern applications. When deciding to use a slotted stator for the design, a combination

of factors including slots, poles, phases and windings need to be employed for obtaining an optimized total machine performance.

For a 3-phase synchronous machine, armature windings are wound such that the number of slots is an integral multiple of 3 [58]. However, the number of slots per pole per phase is not required to be an integer, which means a fractional number of slots per pole per phase is possible, and multiple layers of windings can exist in a single slot. Based on [58], in order to have a balanced voltage in each phase winding, the armature winding should be distributed around the stator periphery in such a way that all 3 phases have the same winding patterns. Therefore, some rules must be followed when designing fractional slots/pole/phase windings of a 3 phase system. As introduced in [58], the fractional part of the slots/pole/phase, when reduced to its lowest level will have a denominator that is not an integral of multiple of 3. For example, $2\frac{1}{2}$ slots/pole/phase is acceptable, while $3\frac{1}{6}$ is not.

The coil pitch of a PMSM is the electrical angle that a single phase winding on the stator stretches across. If the coil pitch is equal to a pole pitch which is always $180°$ in electrical angle, the winding is a full-pitch winding, while if it is less than a pole pitch, the winding is a fractional-pitch winding. During the calculation, this is reflected as the pitch factor, k_p. The pitch factor can be calculated using the following equation

$$k_{pn} = sin\left(\frac{n\alpha}{2}\right) \tag{3.34}$$

where *n* represents the order of the harmonics and α represents the electrical angle spanned by a single phase belt at its fundamental frequency. Without short-pitched design, $\alpha = 180^{\circ}$ and $k_p = 1$. When designing with short-pitched windings, $\alpha < 180^{\circ}$, and $k_p < 1$. By introducing a non-unit pitch factor to the machine, the higher order harmonics could be eliminated. Many practical machines apply fractional-pitch windings with a double layer winding design.

The armature winding of a synchronous machine can be either concentrated wound or distributive wound. Concentrated wound machines have decoupled physical and magnetic characteristics between the phases which tend to increase the rotor eddy current problem due to the armature reaction [43]. With a distributed winding, the stator windings associated with each phase are distributed among several adjacent parts of the slots [59]. In this case, there will be a fractional distribution factor k_d affecting the machine performance. The distribution factor can be calculated by the following equation

$$k_{dn} = \frac{sin\,(\frac{mn\gamma}{2})}{msin(\frac{n\gamma}{2})} \tag{3.35}$$

where n is the order of the harmonics, m is the number of series connected coils per pole per phase, and γ is the slot pitch in electrical radians. The slot pitch is the electrical angular distance between adjacent slots on a stator. Fractional slots per pole per phase and short pitched armature winding design can result in an induced voltage that is nearly sinusoidal and reduced torque pulsations [58]. The product of pitch factor and distribution factor is the winding factor

$$k_{wn} = k_{pn}k_{dn} \tag{3.36}$$

where n represents the order of the harmonics. The winding factor is applied to equation (3.27) to calculate rms back emf. Equation (3.27) can be rearranged to obtain the equation for rms back emf of the fundamental.

$$E_A = \sqrt{2}\pi k_{w1}N_{ph}\phi_{av}f \tag{3.37}$$

In equation (3.37), N_{ph} is the total number of turns per phase, f is the supplying frequency in Hz, and ϕ_{av} is the average magnetic flux which can be calculated from specific magnetic loading

$$\phi_{av} = \bar{B}\frac{\pi d}{p}l \tag{3.38}$$

Although pitch factor causes a small reduction in the fundamental voltage, the higher order harmonics are drastically reduced [59].

3.3.3.5 Core Iron Magnetic Flux Density and Saturation Factor

In practice, core laminations fabricated with ferromagnetic material will start getting saturated as the applied magnetic field intensity reaches a certain amount, and eventually get fully saturated. The magnetization characteristics of a thin-gauge steel, Nippon Steel 15HTH1000 is shown in Figure 3. 6 to illustrate how the magnetization within an electric machine varies with magnetic field strength.

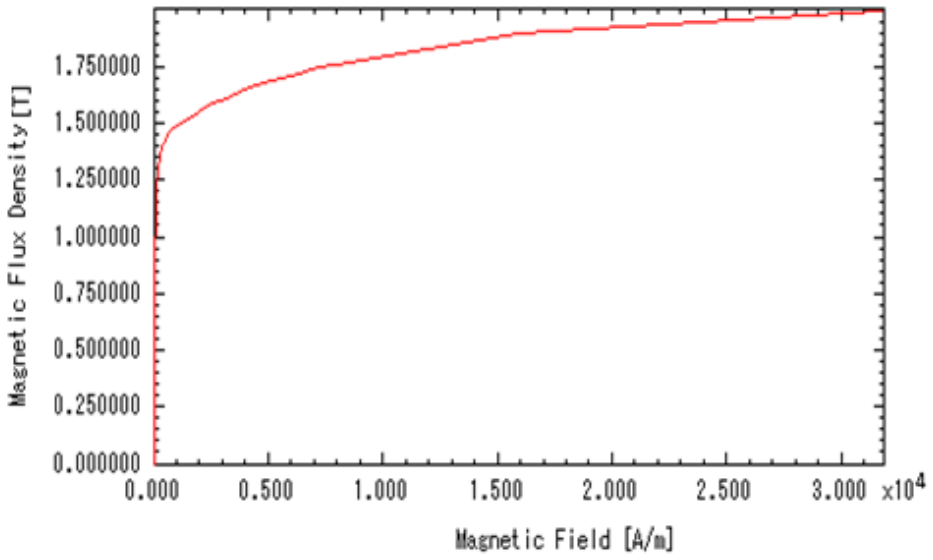

Figure 3. 6 Magnetization B VS. H for Nippon Steel 15HTH1000

As mentioned in the previous section (3.3.3.1), the synchronous machine should be designed to work around the knee of the magnetization characteristics of its core iron. Such loading points are around 1.5 T from the figure. It can be observed from the figure that while the machine is working around the knee, instead of the area before saturation starts, the magnetic flux density will not change dramatically due to a small variation of the magnetic field intensity. In order to avoid excessively large current demand, the loading points should be kept away from heavily saturated area, which is beyond 1.75 T from the figure. The saturation factor is normally used to measure the saturation level of a synchronous machine. The saturation factor is calculated as the ratio of saturated mmf drop along the magnetic flux path over the unsaturated mmf which is just the mmf drop

in air gap since the core iron is assumed to have infinite permeability. The saturation factor also reflects the ratio of the unsaturated machine reactance to the saturated reactance.

3.3.4 Field Weakening

The motor input voltage and current are constrained by the upper limit on the available dc link voltage and current rating of a given inverter. These input voltage and current limits have an impact on 1) the maximum motor speed up to which constant rated torque is available and 2) the maximum torque producing capability of the motor drive system, respectively [60]. Normally, the machine should be operated under the rated speed in order to avoid exceeding the rated voltage determined by the applied inverter. However, in most practical cases, the motor is required to operate within a wide and high speed range that could be beyond its rated speed. According to [61], an extended operating speed range of the PMSM can be achieved by applying field weakening control. Theoretical explanations of this process are also presented in [61]. Field weakening techniques enable the PMSM to run over its rated speed without exceeding voltage and current limits from the available inverter.

As introduced in the previous section "Field Oriented Control", the *d*-axis current $\mathrm{i_d}$ is for rotor magnetic field control. The field weakening technique for the PMSM is implemented by injecting$-i_d$ to the system. It can be observed from equation (3.23) that negative *d* axis current will reduce the magnitude of *d* axis magnetic flux linkage. The field weakening design is usually implemented with fairly large PM flux linkage and winding inductance [62]. Such configurations can help limit the torque current i_q to balance copper losses due to the additional *d*-axis current i_d.

Chapter 4

Design Implementation

Within this chapter, procedures for the PMSM design that are focused on within this thesis are described. Investigations of the existing design are given. Steps for the implementation of the proposed design including initial design and design improvements are presented. The final design performance is presented at the end of the chapter.

4.1 Design Specifications

An existing flywheel system has been designed as an energy storage device for a large commercial hybrid electric vehicle (HEV), taking the place of the traditional chemical battery. A PMSM has been designed to be integrated within this particular flywheel battery as an electric motor/ generator. Based on the experimental analysis of its operation, this existing PMSM design has the following key parameter settings: a relative low magnet magnetic flux linkage (λ_{pm}) of 0.06 [web-T], low inductances of 70 [μH] for both L_d and L_q, and total winding resistance (R) of 8 [mΩ] .

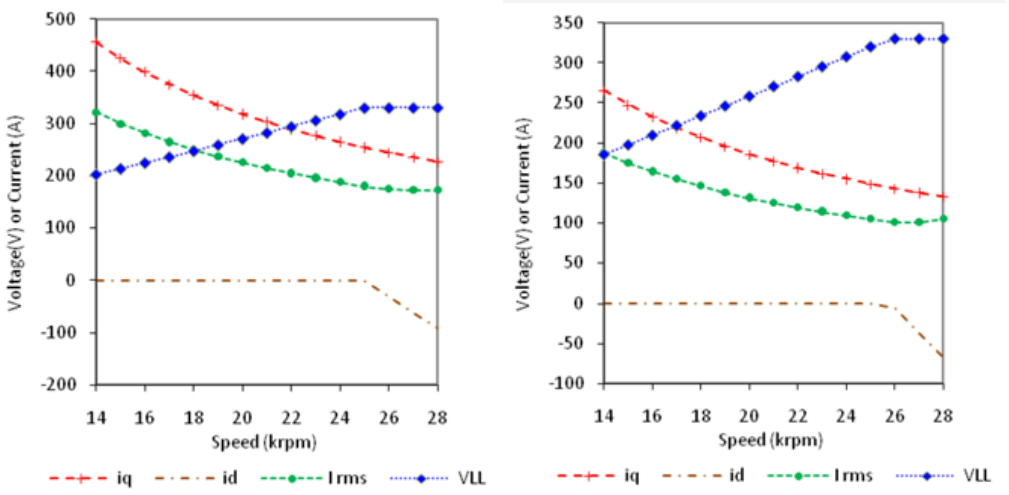

(a) (b)

Figure 4. 1 Voltage and Current Characteristics within the Rated Speed Range for the Existing Design. (a) Motoring at 70 kW. (b) Motoring at 120 kW

With these key parameter settings in place, a spread sheet formula has been written to show voltage and current characteristics from the machine under steady state operation for both rated and over loaded cases. Figure 4. 1 above illustrates the voltage and current characteristics within the typical speed range (14000 rpm - 28000 rpm) of the existing design. The plots are governed by PMSM lumped parameter equations (equations (3.20) to (3.24)) for steady state operation. The figure shows that for both rated and over-rated loading cases, the machine are mostly operating within a constant-flux region, where d-axis current (i_d) is kept at zero. This indicates that no field weakening is applied, and d-axis flux linkage (λ_d) appearing in all lumped parameter equations is simply equal to λ_{pm}. Some issues can be identified from the outputs of such design. As illustrated by the figure, rms current varies significantly with speed. This is not desired for flywheel applications because speed-dependent current will cause the winding ohmic losses to vary with speed. In addition, rms current values from the figure are shown to be large at lower speeds, especially for the over loaded case, and the rms current value at 14000 rpm has exceeded the maximum current limit of 300A that is imposed by the applied inverter.

The existing flywheel battery requires a new design of PMSM with improved voltage and current characteristics together with a constant and high average of efficiency within a wide operating speed range. In addition, the new machine is also required to be designed to fit into the existing flywheel system for mobile applications. Such requirements places an increased number of constrains on the design, including physical dimensions and maximum limit of DC link voltage from the commercial inverter. Detailed design specifications are listed in Table 4. 1.

Speed Range	0 — 28000 rpm
Typical Operating Range	14000 – 28000 rpm
Typical Operating Frequency Range	467 – 933 Hz
Poles	4
Target Motor Average Efficiency	> 98% at Rated Power
Target System Average Efficiency	> 95% Include Inverter Loss
Phase – Phase EMF THD	< 1.32%
DC Link Voltage	600 V
DC Link Range	500 – 700 V
Rated Continuous Power	70 kW
Overload Power 30s at least	120 kW
Stator Outside Diameter	9.01 in (229 mm)
Height	5.66 in (144 mm) including end windings

Table 4. 1 Proposed PMSM Design Specifications

By inspection, speed-dependent current from the existing design output arises and is due to the relatively low magnet flux linkage design. Equation (3.10) indicates that for a certain power demand, the machine requires a large torque at lower speed operations. Since the existing design has been configured such that $L_d = L_q$, torque (τ) in equation (3.25) is determined by the product of λ_{pm} and i_q only. Therefore, with a relative small value of λ_{pm}, a large value of i_q is required to gain sufficient torque, resulting in large joule losses in the winding

circuit at lower speeds. As the speed increases, the torque demand decreases for the same power rating, and the value of i_q decreases to reduce the torque. The rms current shown in Figure 4. 1 is calculated from i_d and i_q as

$$I_{rms} = \sqrt{\frac{(i_d{}^2 + i_q{}^2)}{2}} \tag{4.1}$$

It can be observed that while keeping $i_d = 0$, the rms current is influenced by only i_q, and will vary with speed in the same manner as i_q does.

In order to improve the current characteristics in the existing design, a decision has been made to design a new machine with increased λ_{pm} and more region of field-weakening operations within the typical speed range. As mentioned above, since torque is designed to be influenced by the product of λ_{pm} and i_q only, larger value of λ_{pm} can keep i_q smaller, thus minimizing joule losses, especially at lower-speed regions where larger torque is demanded. However, large λ_{pm} translates to large d-axis flux linkage λ_d, and will result in a significant increase of q-axis voltage (v_q) in equation (3.20) due to the speed term "($\omega_r \lambda_d$)". For steady state operations, the reference speed ω_r is equal to the synchronous speed ω_e . Similar to the rms current calculation, the peak phase voltage can be calculated from v_d and v_q as

$$\hat{V} = \sqrt{(v_d{}^2 + v_q{}^2)} \tag{4.2}$$

As the operating speed increases, the value of v_q will increase to a point where $\hat{V}$ reaches the voltage limit imposed by the inverter. The system voltage must not exceed the rated value, and for the machine to run further within the extended speed range, negative values of *d*-axis current ($-i_d$) must be injected into the system to invoke field weakening. Within the region of field-weakening operations, λ_d decreases as speed increases while peak phase voltage is kept constant at the rated value.

Based on equation (4.1), the injected $-i_d$ will add magnitude to I_{rms}. This indicates that i_d counteracts i_q, and a profile of a more constant I_{rms}, without

dependence on the speed, could be achieved. However, if the machine has been designed with an extremely large λ_{pm}, the operation requires much more field weakening, that is, a significantly large $-i_d$ to maintain rated voltage. In this case, $-i_d$ will take the position of i_q to dominate the operating performance of the machine, and will produce significant amount of joule losses in the winding circuit. This is especially true for higher speed regions since v_q in equation (3.20) increases with "$(\omega_e \lambda_d)$". This will result in a significant increase of I_{rms} in higher speed regions. Therefore, the design goal is to increase λ_{pm} from the existing design until a value that has more constant I_{rms} profile can be obtained. In order to limit the current values, designing the machine with increased inductances (L_d and L_q) has also been favored. The influence of the inductance is indicated by flux equations (3.23) and (3.24).

4.2 Initial Design

As mentioned in the previous chapter, the design of the PMSM should not be isolated from its bearing system and inverter system design. For the design described in this thesis, a high speed ball bearing is used, rather than active magnetic bearings. Compared to active magnetic bearings, a ball bearing is less expensive and has less control complexity. Therefore, for hybrid electric vehicle applications where flywheel system only operates as a short term kinetic energy recovery device, ball bearings appear to be more effective solutions in aspects of cost and control. To apply the design implementation to a practical mobile system, a decision of using a commercially available inverter design was made during the beginning of design process. The available inverter, "SKAI" is designed with water-cooling system, and is capable of a 150 kW power, a 300A rms current and a 15 kHz switching frequency. It is shown in Table 4. 1 that the proposed PMSM is to be designed with a high operating frequency. This means that a high switching frequency from the applied inverter is required. Thus, in order to balance the system losses due to the high switching frequency, the proposed PMSM should be designed with low rms current demand.

As introduced in chapter 3, some design parameters need to be predicted at the beginning of the entire design process. Initially, the key parameters of specific magnetic loading, $\bar{B}$, and specific electric loading, $\bar{J}$ were set to be 0.46 T and 44000 A-T/m, respectively. By referring to the standard value range which is mentioned in section 3.3.3.1, it can be observed that a relatively low specific magnetic loading has been used for the initial design. Such an approach can lead to a number of design advantages for flywheel applications including low iron losses and eliminated stator winding losses while freewheeling [19]. A number of other parameters for the initial design are also required to be determined. The values for all key initial design parameters of the PMSM design described in this thesis are listed in Table 4. 2.

Specific magnetic loading, T	0.46
Specific electric loading, A-T/m	44000
Rated line-line voltage, V	360
Current density, A/mm^2	7
Air gap length, mm	2.5
Number of poles	4
Number of slots	30
Number of winding layers	2
Wiring type (Delta or Y)	Y
Short slot pitch, slot	1
Slot width partition (of the total width of one tooth-slot)	60%
Rotor type	SMT
Residual Flux Density (Br) of selected PM, T	1.12
Type of the core iron material	Nippon Steel 15HTH1000
Desired magnetic flux density at stator tooth, T	1.15
Desired magnetic flux density at stator back core, T	1.45

Table 4. 2 List of Key Design Parameters

The above parameters have formed the initial entries to the design spread sheet. Starting with these entries, other design parameters can be calculated by applying design principles and equations, which have been introduced in chapter 3. The initial design process has been preceded according to the following steps, and all calculations listed below are calculations behind the design spread sheet:

1. With the values of rated power, rated speed (typically 14000 rpm) and predicted $\bar{B}$ and $\bar{J}$, the radius of the mean air gap can be calculated from the first principle equation (3.32)
2. With the calculated mean air gap radius and the pre-determined air gap length, the radius of the inner surface of stator can be determined; since the outer diameter of the machine has been given as a requirement, the stator lamination depth can be calculated
3. The winding factor for the fundamental is calculated by using equations (3.34)–(3.36); all required variables have been determined and listed in Table 4. 2
4. Rated phase voltage is calculated from the given rated line-line voltage; with the rated phase voltage, the total number of winding turns per phase (N_{ph}) can be calculated by equation (3.27) after rearrangement
5. The number of coils per phase is determined by the number of slots, the number of layers and the number of phases; the turns per coil N_T is then calculated with the number of coils per phase and N_{ph} from the previous step; the rounded value is used for the further calculations
6. The rated phase current is determined by the rated power and the rated phase voltage from step 4; with phase current value, N_T from step 5 and the pre-determined current density, the slot area can be calculated
7. Slot width can be calculated based on the slot width partition from Table 4. 2; the slot depth can then be calculated with slot width and slot area from last step by assuming rectangular shape

At this point, the outline of the machine stator is complete. Figure 4. 2 shows the outline of the stator from the initial design for the proposed PMSM. In order to obtain a reasonable design, iterative procedures are inevitable due to the fact that many parameters have to be estimated at the beginning. The judgment of the quality of the design can be made based on observations from the figure. For example, the space of back cores appears sufficiently large to conduct magnetic flux without being over saturated; the stator tooth width appears sufficiently long to avoid structural failure (consider that multiple winding turns are held by the tooth structure).

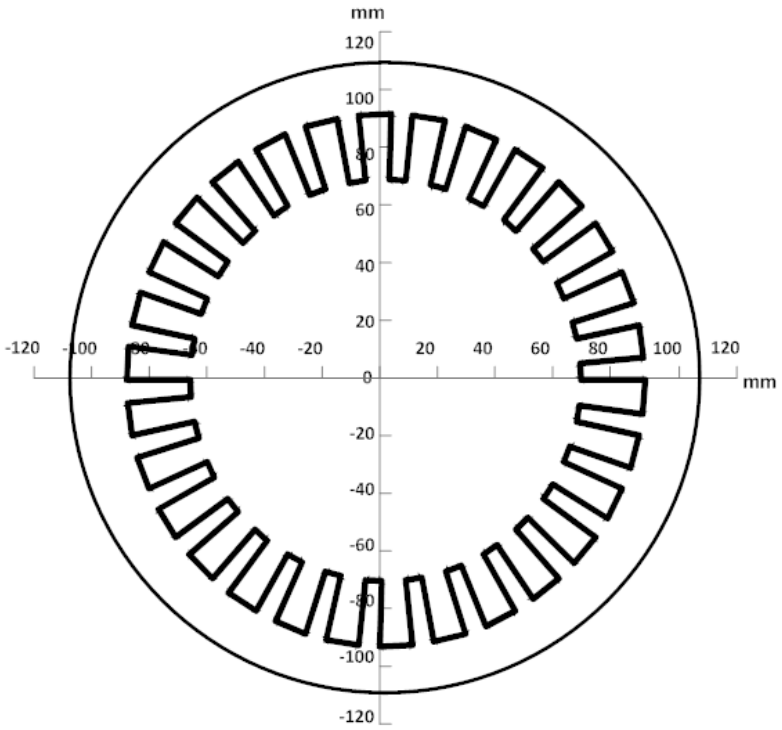

Figure 4. 2 The Outline of Stator of the Initial Design

The rotor design procedures are listed in the following steps:

8. Desired peak magnetic flux density at stator tooth ($\widehat{B}_t$) and back core ($\widehat{B}_c$) are both pre-determined as shown in Table 4. 2, and those corresponding peak magnetic field intensities ($\widehat{H}_t$ and $\widehat{H}_c$) can be determined by looking up the figure of the characteristics for the selected lamination materials (Nippon Steel 15HTH1000)

Since magnetic field intensities at all air, stator tooth and stator back core are all known, the total saturated mmf drop along the magnetic flux path can be calculated by magnetic circuit equation below

$$mmf = \hat{H}_{mag} l_{mag} = \hat{H}_{airgap} l_{airgap} + \hat{H}_t l_t + \hat{H}_c l_c \quad (4.3)$$

In equation (4.3), mmf stands for the total magneto motive force required from an applied magnet, *H* is magnetic field intensity and *l* is the flux path.

9. The peak magnetic field intensity of selected permanent magnet $\hat{H}_{mag}$ can be determined by looking up the magnetizing characteristics of the selected magnet, same as the example shown in Figure 3. 5; $\hat{H}_{mag}$ at the operating point is calculated with remanence, *Br* and air gap loading, $\bar{B}$; l_{airgap} and l_t have been determined, and l_c can also be estimated from the stator structural; therefore, the thickness of the PM, l_{mag} can be calculated from equation (4.1)
10. Since the SMT type of rotor is chosen, the radius of the rotor lamination is simply determined as starting from the central axis to the inner surface of magnets

During step 9, some assumptions are made for calculations. First, the magnetic flux crossing the air gap is assumed to pass through the stator tooth only, which means there is no flux leakage existing. Second, after passing the tooth area, the magnetic flux splits equally at the back core. After accomplishing step 10, essential configurations for the initial design have been set, and all initial parameters and calculated variables will be used as boundary conditions to create 2-D FEM model for simulations.

The 2-D model of the PMSM for the initial design is created by using commercial software JMAG. Electromagnetic field analyses are carried out by applying finite element analysis (FEA) with JMAG. Simulations are run in steady state mode for open circuit, rated power load of 70kW and over-rated power load of 120kW. The interested speed range (14000 rpm - 28000 rpm) is divided into 15

speed cases, and FEA calculations by JMAG is carried for each speed case for all three loading conditions mentioned above within a single iteration. Various aspects of outputs from simulations including open circuit voltage, inductances, magnet flux linkage, and machine losses from each speed case are collected for further analysis.

Macro scripts are created with spread sheet to implement functions for field weakening operations over the typical speed range that is divided into 15 speed cases, the same speed cases as being used for FEA analysis. Values of key parameters magnet magnetic flux linkage (λ_{pm}) and inductances (L_d and L_q) that have been returned by FEA are used as inputs to the spreadsheet to determine steady state voltage and current characteristics of the machine as shown in Figure 4. 1. Open circuit voltage waveforms are exported from JMAG and then input to Matlab for the analysis on their harmonic spectrums. Investigations are also carried out on many other outputs from JMAG simulations including torque waveforms, magnetic flux distributions and machine losses. Combined investigation results from various aspects of the initial design guide the design to its improvements.

4.3 Design Improvements

4.3.1 High Magnet Magnetic Flux Linkage Design with More Field Weakening

Magnet magnetic flux linkage, λ_{pm} has a big impact on the performance of PMSM. This is reflected by the fact that λ_{pm} appears throughout lumped parameter equations as key variables for analytical analysis. Voltage and current characteristics from steady state operations for the existing design have been shown in Figure 4. 1. As mentioned in section 4.1, the goal is to re-design the machine with an increased λ_{pm} to improve the rms current characteristic from the existing design. In order to approach to the right value of λ_{pm} for the design, the same steady state analysis process with field weakening operations within rated

speed range are carried out for different values of λ_{pm} by making λ_{pm} slightly increased. Three different values of λ_{pm} (0.08, 0.1, 0.12 Wb-T) being investigated were chosen to demonstrate the effect. Much higher machine inductances of 300 μH for both L_d and L_q have been chosen, because during the design improvements, decision has been made to design the machine operating at points without much saturation to reduce current demands. It should be noted that a PMSM designed with a large effective air gap is typically unsaturated under all reasonable operating conditions. Therefore, L_d and L_q can be considered to be relatively large and constant over the operating range (rotor saliency is negligible and L_d=L_q) [19]. Other variable settings are: DC link voltage (600V), winding resistance (8mΩ), and constant power rating (70 kw).

For all three values of λ_{pm}, the values of efficiency within the nominal speed range (14 krpm – 28 krpm) are plotted. Iron losses are neglected for this analysis because the goal is to determine the optimized value of λ_{pm} by observing behaviors of i_d and i_q during the operation within nominal speed range. Therefore, during this investigation, the machine efficiency is only affected by Ohmic losses from the stator windings.

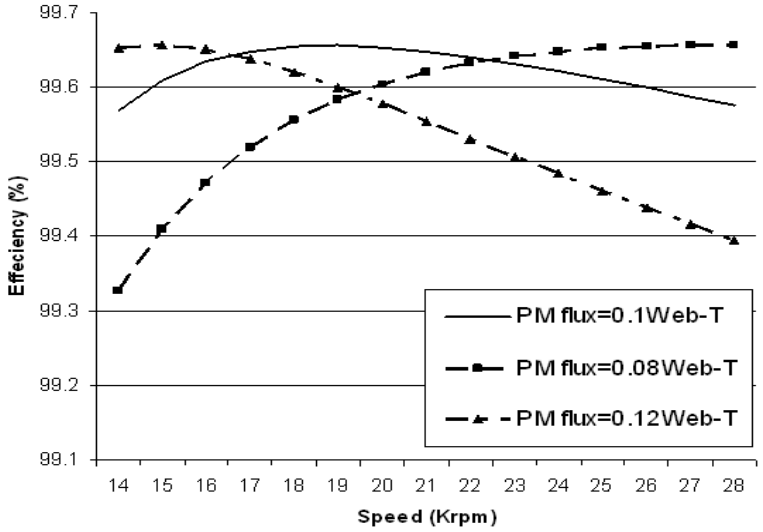

Figure 4. 3 Output Efficiency (Neglecting Iron Loss) At Constant 70 kW within Typical Speed Range With Different PM Flux Linkages

The behavior of the output efficiency shown in Figure 4. 3 is governed by PMSM lumped parameter equations. The phenomena that the curve changing with the value of λ_{pm} has been explained in section 4.1 based on lumped parameter equations. By inspecting Figure 4. 3, if the magnet magnetic flux linkage is too small which is the case shown by the curve with λ_{pm}=0.08 Wb-T, additional current (i_q) is required at lower speeds, resulting in large joule losses and low efficiency. In contrary, if the magnet flux linkage is too high which is the case shown by the curve with λ_{pm}=0.12 Wb-T, more field weakening is required at higher speeds, resulting in increased joule losses due to the injected $-i_d$, hence the efficiency is reduced. However, before λ_{pm} reaches an extremely high value as 0.12 Wb-T, a nearly constant efficiency curve can be obtained as shown by the curve with λ_{pm}=0.1 Wb-T. Such efficiency curve indicates a nearly constant rms current characteristic within the typical speed range from the design.

During iterative design approach, some initial design parameters are re-configured in order to have λ_{pm} increased. Steps involved for the improvement include replacing the permanent magnet with stronger ones and increasing magnet thickness together with the air gap length being enlarge. The design approach has resulted in a final design with a magnet magnetic flux linkage of 0.102 Wb-T. The voltage and current characteristic from the final design output will be presented in later section of the chapter along with the other final design results.

4.3.2 Design Tooth-Tips to Reduce the Cogging Torque

Large spaces between stator teeth and slots can result in the variation of air gap permeability, that is, the air gap reluctance varies as a function of the angle. This is not desired because the cogging torque increases with the air gap reluctance changing rate, which is reflected by equation (2.6). To reduce the variation of the air gap permeability, and hence to reduce the cogging torque, tooth-tips design to the stator teeth has been applied for design optimizations. By applying such strategy, stator teeth widths (w_t) have been made much longer than the slots widths (w_s) nearing to the inner stator surface. Comparisons between two

designs, the one with the tooth-tips for the teeth and the one without are illustrated in Figure 4. 4.

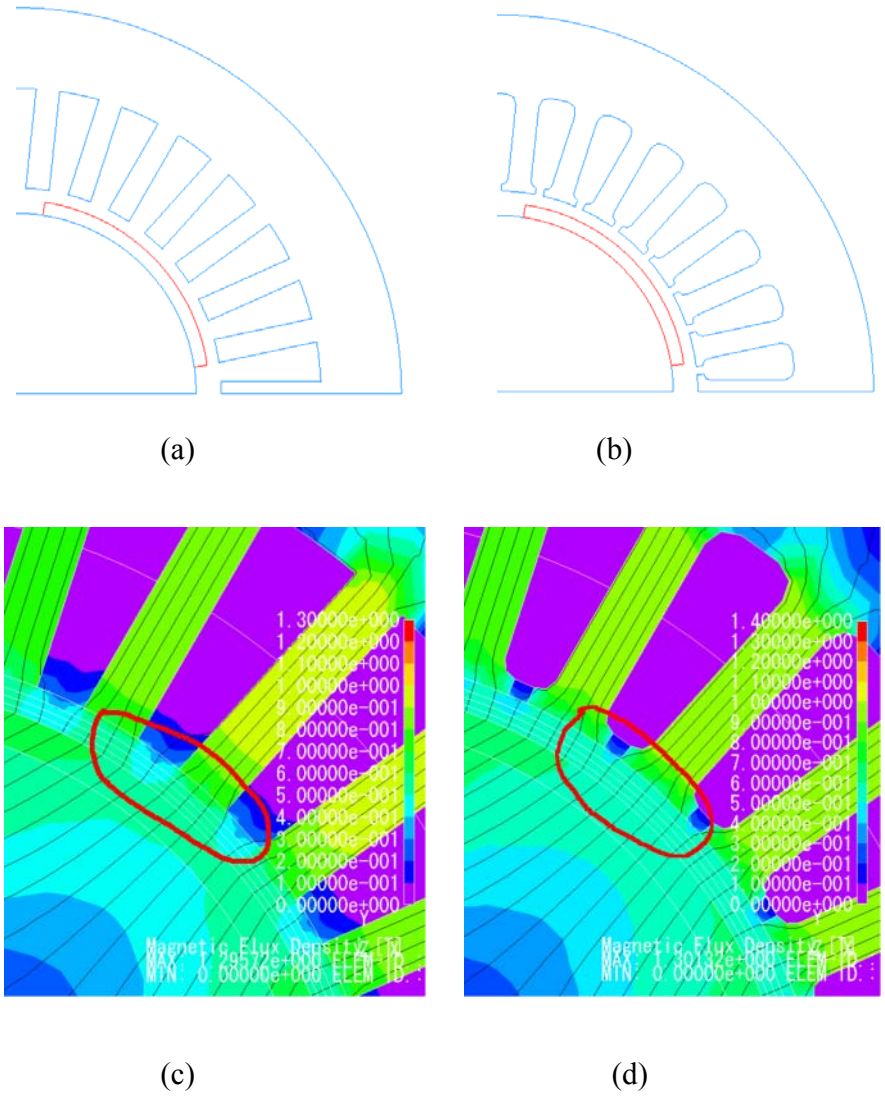

Figure 4. 4 Comparisons between two slot-tooth designs (a) Slot-tooth structure without tooth-tip design. (b) Slot-tooth structure with tooth-tip design. (c) Magnetic flux distribution for design (a). (d) Magnetic flux distribution for design (b)

Figure 4. 4 (a) and (b) show how the outline differs by applying tooth-tip to the stator slot-tooth. (c) and (d) show the magnetic flux distributions near to the slot openings by FEM analysis for both designs. The time-stepped finite element (FEM) analysis was carried out for steady state operation at typical speed of 14 krpm and 70kW loading. It can be observed from the figure that design (b) has a

more uniform magnetic flux distribution along the air gap during the operation, which means that uniform air gap permeability has been achieved due to the tooth-tip design being applied to the stator slot-tooth.

Output torque waveforms are also plotted for both designs under the same initial conditions to illustrate the effects due to the tooth-tip design. The plots were made by using JMAG, and are displayed in Figure 4. 5. It can be seen from the figure that the design with the tooth-tips gives a smoother torque wave form, less noise and a higher average magnitude. This indicates that, by applying tooth-tip structure design to the initial design of the PMSM, cogging torque has been successfully reduced.

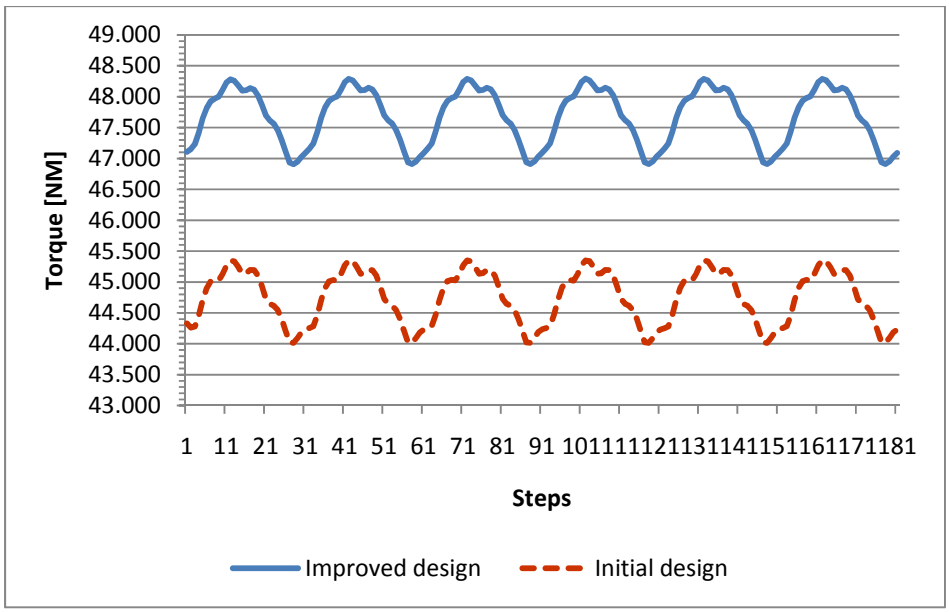

Figure 4. 5 Torque Waveforms from Two Proposed Designs (a) Slot-Tooth Structure without Tooth-Tip Design. (b) Slot-Tooth Structure with Tooth-Tip Design

An increased slot leakage inductance could be a negative effect due to the tooth tips. As a consequence, the total winding inductance will increase, which will limit the current building up rate due to the transient or fault. FEA analysis from JMAG has shown non-salient inductances along *q* and *d* axis as high as 400 μH for the optimized design.

4.3.3 Influence of Magnet Arc Length on THD

As described in Table 4. 2, the initial design has been implemented with fractional short-pitched distributed winding design. There are 30 stator slots being assigned for the 4-pole machine. Armature windings are inserted into slots with 2 layers, and distributed with 1-slot short pitch. Figure 4. 6 illustrates one half of the stator structure with winding distribution layout for the proposed PMSM design.

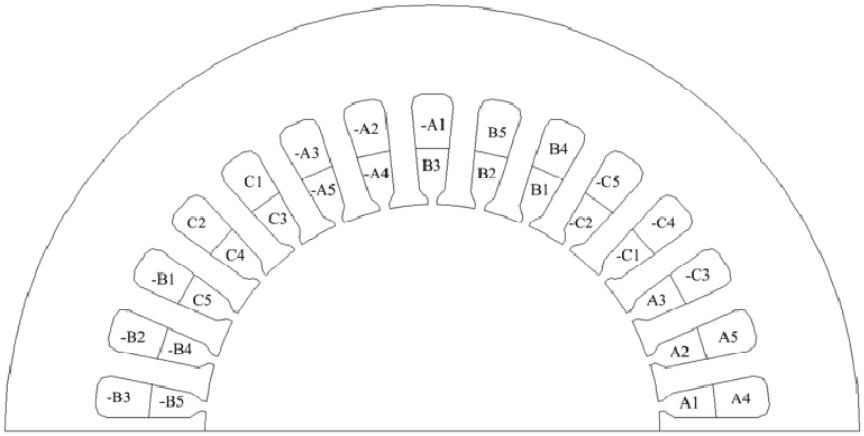

Figure 4. 6 Fractional-Slot Distributed Winding Layout for Initial Design

Other slot-winding designs have also been considered. For example, the first initial design was configured as a 4-pole machine with a 24-slot distributed winding without short pitch. Calculations show that such winding design has a winding factor less effective than the one given by the proposed design which has a 1-slot short-pitch. As introduced in chapter 3, winding factor is the product of pitch factor and distributed factor, and is calculated from equations (3.34)-(3.36).

Fractional winding factor can significantly reduce higher-order harmonics from open circuit EMF, hence results in reduced open circuit THD of EMF. THD of the back EMF or open circuit induced voltage is calculated as the ratio of "total rms of all the harmonic components" over the "fundamental".

$$V_H = \sqrt{\sum_{n=2,3,4,\ldots}^{n\to\infty} {V_n}^2} \tag{4.4}$$

$$\text{THD} = \frac{V_H}{V_1} \times 100\% \tag{4.5}$$

V_H and V_n in equation (4.4) represents the rms of all the voltage harmonic components and the nth voltage harmonic, respectively. V_1 in equation (4.5) represents the fundamental of the voltage. It can be shown that the Fourier series of a squire wave function within the domain of [0, π] is calculated to be

$$F_n = \frac{2\hat{F}}{n\pi}\sin(n\theta_e) \tag{4.6}$$

where F_n represents the nth harmonic of the squire wave function, $\hat{F}$ is the peak value and θ_e is the variable of electrical angle within [0, π].

The mmf function produced by an ideal radial - magnetized magnet with an arc length of θ_m can be assumed to be a squire wave function. θ_m is mechanical angle. For the proposed machine design with 4 poles, the angle value in electrical is equivalent to half of the angle value in mechanical which means that the electrical angle domain of [0, π] is reflected by the mechanical angle domain of [0, π/2]. This domain is actually the one that is spanned by a single magnet pole with full magnet arc length. By inspection, the magnitude of all harmonic components from the mmf function produced by a single pole magnet with an arc length of $\theta_e/2$ can be calculated from equation (4.6). Calculating results from different arc lengths can be compared to determine the one that will result in improved output with significantly reduced open circuit THD of induced voltage.

Table 4. 3 shows calculated winding factors of the principle and higher harmonic components (k_{wn}) up to the 25th harmonic for the initial design. Fourier series equation (4.6) indicates that the magnitudes of all harmonic components from a squire wave function are attenuated by the factor of $1/n$. Therefore, in order to reflect the direct influence to harmonic components from winding factors, calculating results on the ratio k_{wn}/n are also shown in Table 4. 3.

n	1	5	7	11	13	17	19	23	25
k_{wn}	0.9567	0.2	0.1495	0.1095	0.1022	0.1022	0.1095	0.1495	0.02
k_{wn}/n	0.9567	0.04	0.0214	0.001	0.0078	0.0060	0.0058	0.0065	0.0008

Table 4. 3 Calculated Winding Factors for Initial Design

The calculating results of winding factors indicate that by employing short-pitched fractional distributed winding design, the higher harmonics from the output of the initial design have been significantly reduced with a small amount of magnitude lost from the fundamental. Such design has gained benefits including low THD, less operating noise, reduced iron losses and increased total efficiency. However, the inspection on the harmonic spectrum of the open circuit back EMF shows that the 5^{th} and the 7^{th} harmonics still appear significant, and the open circuit THD is still predicted to be as high as 2.43% which does not meet the design requirement. Therefore, in order to further reduce the THD, decision has been made to improve the machine with reduced magnet arc length.

Such designing idea came out from the inspections on Fourier series equation (4.6). It can be observed that for a particular harmonic component *n*, its magnitude can be eliminated by giving a certain value of θ_e. Plots have been made based on equation (4.6) for the absolute values of fundamental magnitude and relative magnitude of the 5^{th}, 7^{th}, 11^{th} and 13^{th} harmonics. The peak value of the function $\hat{F}$ has been assumed to be 1, and harmonic components higher than 13^{th} have been ignored since they are not primary components. Plot results are shown in Figure 4. 7

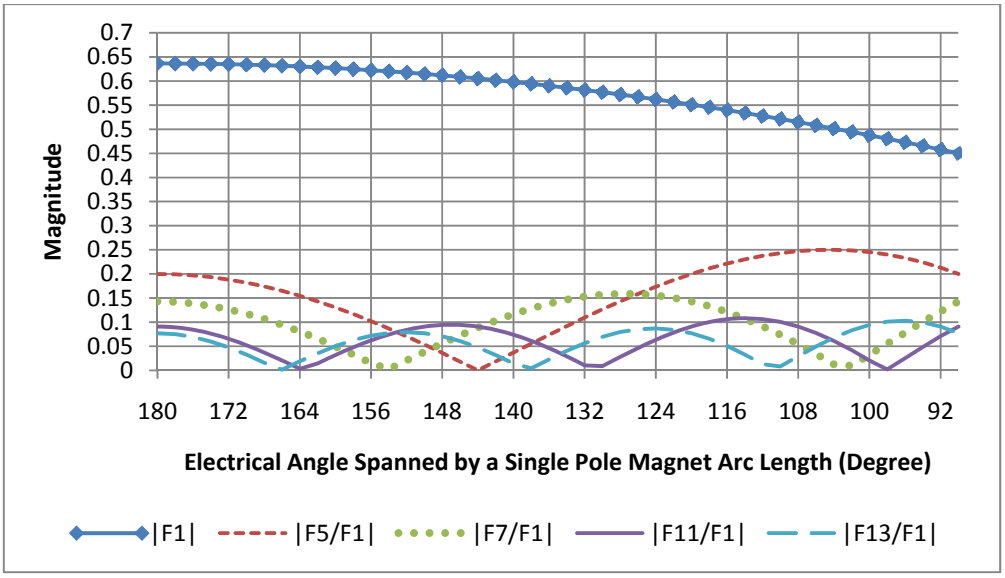

Figure 4. 7 Absolute Magnitude of Fundamental and Relative Magnitude of Higher Harmonics VS. Electrical Angle Spanned by a Single Pole Magnet Arc Length

Figure 4. 7 illustrates behaviors of those harmonic components from a squire wave function as the electrical angle being reduced from 180 degree to 90 degree. It can be observed from the plots in the figure that higher order harmonics drop quickly to zero as the magnet arc length being reduced, while in contrast, the fundamental magnitude decreases slightly. In order to designing with a more accurate magnet arc length for the machine, plots have also been made for relative magnitudes of the same harmonic components (the 5^{th}, 7^{th}, 11^{th} and 13^{th}) by taking account of the winding factors calculated in Table 4. 3.

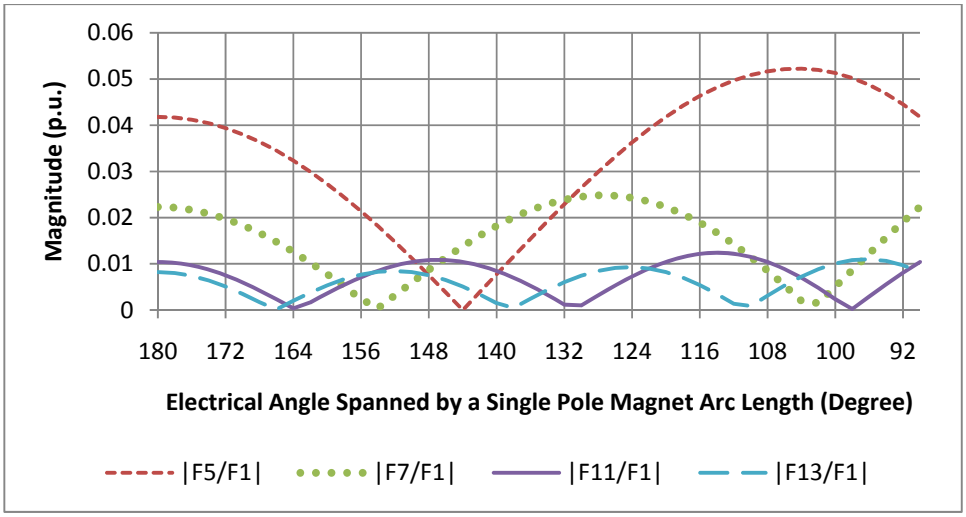

Figure 4. 8 Absolute Relative Magnitude of Higher Harmonics VS. Electrical Angle Spanned by a Single Pole Magnet Arc Length Including Winding Factor Effect

It can be seen from the figure that magnitudes of the 5th and 7th harmonics are significant. By inspection, THD can be reduced if designing the magnet arc length such that it spans an electrical angle where either the 5th or the 7th harmonic shows a magnitude closing to zero from the curves in Figure 4. 8. It can be observed that at the electrical angle of about 144 degree, the 5th harmonic component which carries the most significant amount of relative magnitude among all higher harmonics could be eliminated. The trend of THD output curve varying with electrical angle have also been plotted to help determine the best magnet arc length for theoretically the lowest THD.

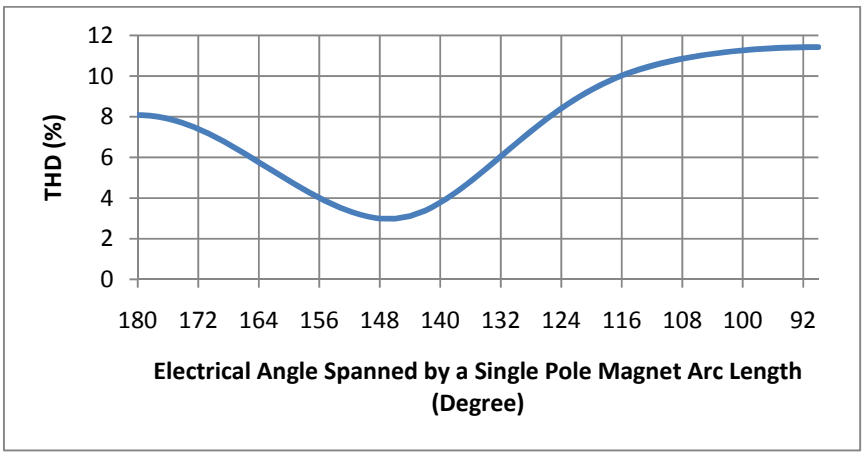

Figure 4. 9 THD VS. Electrical Angle Spanned by a Single Pole Magnet Arc Length Including Winding Factor Effect

Figure 4. 9 shows that the THD drops to the lowest value at the electrical angle of about 146 degree, which is in equivalent to a 73 degree mechanically. Therefore, a decision has been made to design the magnet with an arc length of 73 degree mechanically for each single pole.

Structures of magnets for one pole of the machine from both full arc design (initial design) and reduced arc design are shown in Figure 4. 10 below.

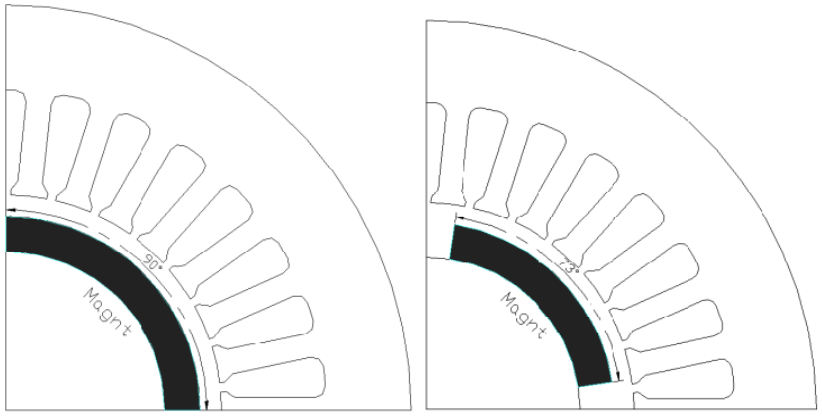

(a) (b)

Figure 4. 10 Structures for Two Magnet Designs. (a) 90 Degree Full Arc Design, (b) 73 Degree Reduced Arc Length Design

Time-stepped 2D FEA for both designs have been carried out. Open circuit back EMF waveforms for both cases were plotted, and data were collected for Fourier analysis with Matlab. The harmonic spectrum of open circuit voltage has been plotted for both cases, and comparisons are presented in Figure 4. 11.

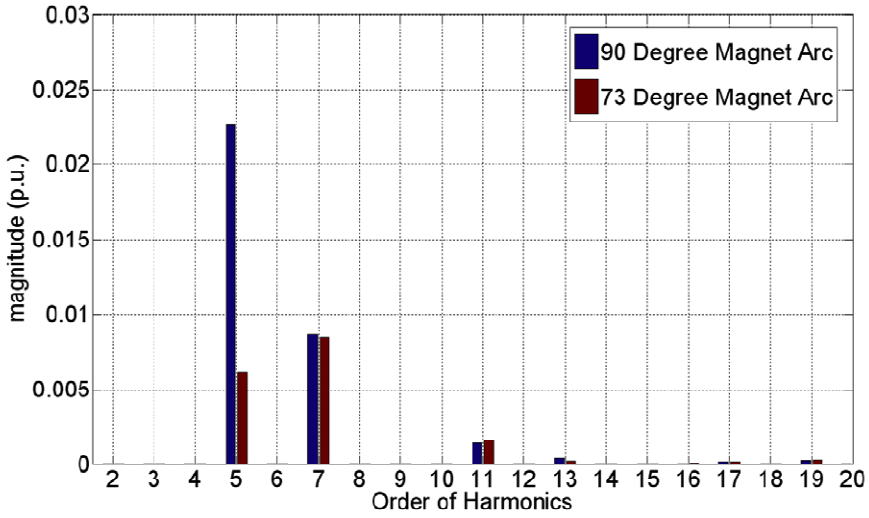

Figure 4. 11 Comparisons of Back EMF Harmonics Spectrums for Two PMSM Designs

The figure clearly shows that the 5th harmonic of the back EMF has been significantly reduced due to the reduced magnet arc design. The calculated results also revealed that the THD has been successfully reduced from 2.31% from the initial design to 1.103% which is imposed by the improved design.

4.4 Final Design Results

After an iterative process combining analysis and improvements on the initial design, the final design that has successfully met all design requirements has been obtained. The structural details are included in Appendix A, while parameter settings and output performances in various aspects are presented in this section.

2-D time stepped FEA were carried out for magnetic flux analysis and machine losses analysis by using JMAG. Analysis has been applied for steady state operation within typical speed range for all open circuit, rated loading and over rated loading conditions. The JMAG output for the open circuit case is shown in Figure 4. 12 with steady state operation under rated speed 14000 rpm.

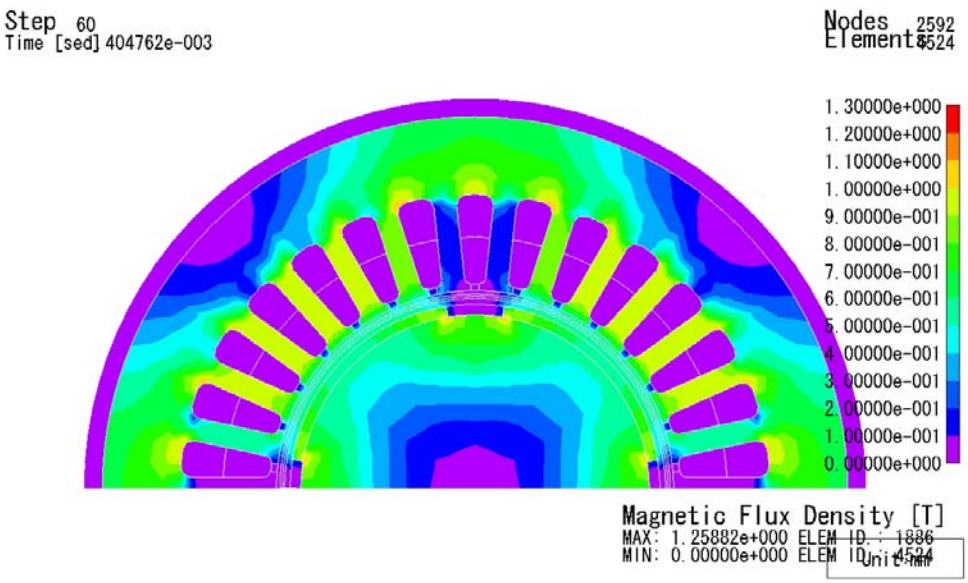

Figure 4. 12 Magnetic Flux Density Distribution within the Machine at 14000 rpm, Open Circuit

It can be seen from Figure 4. 12 that magnetic flux density along the air gap is about 0.5 T which is closing to specific magnetic loading that have been predetermined during the initial design. The air gap magnetic flux density is also uniformly distributed, resulting in reduced harmonics and less rotor losses in the output results.

Calculations by FEA show that the final design has a magnet magnetic flux linkage (λ_{pm}) of 0.102 [Wb-T] and inductances with non rotor-saliency ($L_d = L_q$) of 400 [μH]. With such parameter settings, the analytical analysis by spread sheet returns the following figure showing voltage and current characteristics together with output efficiency (without considering iron losses) under rated loading (70kW) within the typical speed range.

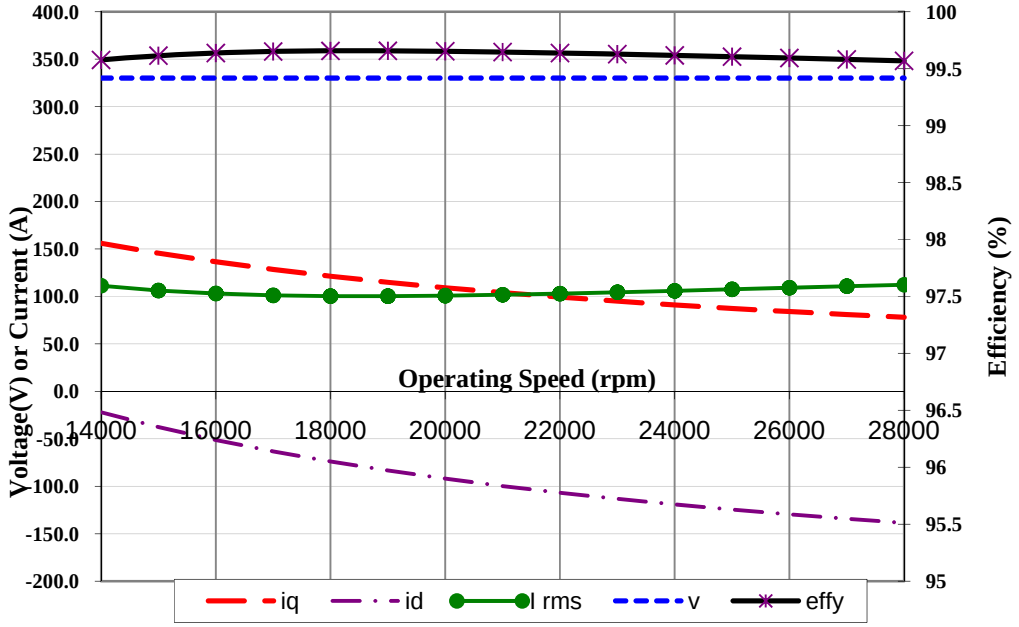

Figure 4. 13 Voltage and Current Characteristics and Efficiency Output within Rated Speed Range for the Final Design (Without Iron Losses), Motoring At 70 kW

By comparing the outputs to those from the existing design shown in Figure 4. 1 (a), it can be observed that the final design has applied an extended field weakening region within the typical speed range. The rms current from the final design has been kept as low as about 100 A throughout the speed range, without significant variation due to the speed. The output efficiency without considering iron losses is kept almost constant with an average value as high as about 99.6%.

Machine losses from the final design have been calculated by FEA with JMAG, as well. Results for 70 kW loading case were plotted in Figure 4. 14. The components that have been considered for losses analysis are rotor and stator laminations and permanent magnets.

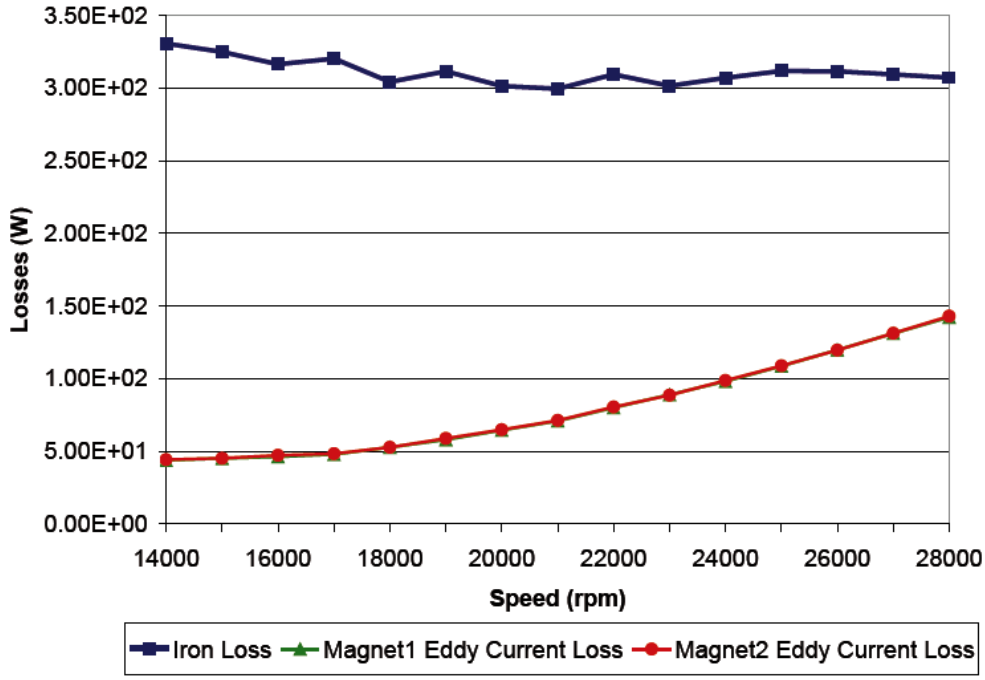

Figure 4. 14 Iron Losses and Magnet Eddy Current Losses within Typical Speed Range, Motoring at 70 kW

It is shown in the figure, that throughout the typical speed range, the iron losses from rotor and stator are kept almost constant as 310 W. This has indicated that under field weakening conditions, the iron losses do not change significantly. However, the eddy current losses in the magnets do increase with speed. This total increased amount of losses is shown to be as high as 100W. Since it is a 4 pole machine, there are 2 magnet sets being examined (one for each pole pair). Because all magnets are symmetrically mounted along the rotor surface, eddy current losses from both magnet sets are expected to be the same, as shown by those overlapping curves from Figure 4. 14.

With calculated iron losses and magnet eddy current losses in place, the total efficiency of the final design can be predicted more accurately. The same analysis process has also been carried out for 120 kW over rated loading case. Final results for both loading cases are presented in Figure 4. 15

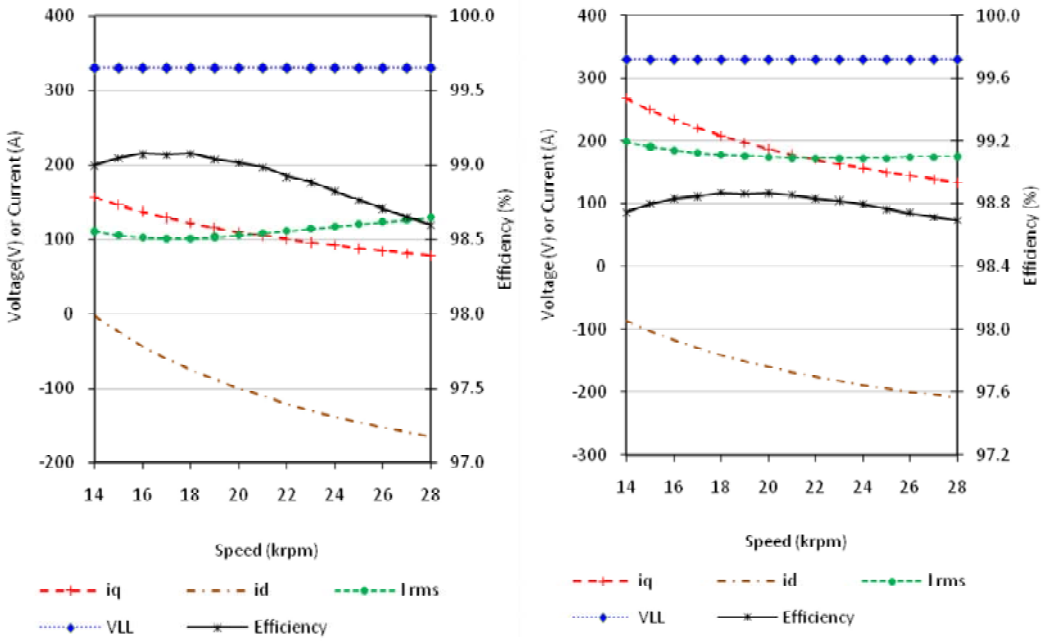

(a) (b)

Figure 4. 15 Final Performances within Rated Speed Range. (a) Motoring at 70 kW. (b) Motoring at 120 kW

It is shown in Figure 4. 15 that by considering all copper losses, iron losses and magnet eddy current losses, the final design is capable of operation within typical speed range with an average efficiency in excess of 98.5% under 70 kW load condition, and in excess of 98.4% under 120 kW over load condition. Field weakening are applied throughout the typical speed range for both cases. A total harmonic distortion (THD) of open circuit back emf has been kept as low as 1.103%. Figure 4. 15 also indicates that the rms current limit of 300A which is imposed by the available power electronic converter is not exceeded under both rated and over load conditions. The current profile within the typical speed range is kept almost constant, and has an average value of 112A for the 70 kW rated loading condition and an average value of 189A for the 120 kW over-rated loading condition. There is only a standard deviation of less than 10A (about 8.9%

for 70 kW loading condition and about 5.29% for 120 kW loading condition) from the current profile for each of those two cases.

To summarize, the final improved design shows great characteristics that have successfully met all design requirements in various design aspects including electrics, electromagnetic and mechanics.

Chapter 5

Conclusion and Future Work

This thesis presents an approach to design a high speed permanent magnet synchronous machine suitable for integration in a flywheel energy storage system within a large commercial electric vehicle (HEV). Design challenges due to the high speed application, including iron losses, cogging torque and total harmonic distortion have been investigated. The existence of the flywheel system has placed additional constrains to the design. The machine has to be designed to meet all requirements listed in Table 4. 1.

The first principle and related design equations were reviewed. The initial design was carried out by using an iterative approach that combines analytical lumped-parameter performance analysis with 2-D finite element analysis (FEA). Selected design strategies from previous work were also reviewed and applied to obtain the final design. The final design has been implemented with extended field weakening region, and it shows great performance throughout the typical speed range (14000rpm – 28000rpm). The average value of the total efficiency is over 98%, and rms currents are kept lower than the limit with only small variations due to the speed for both rated and over-rated loading conditions. The total harmonic distortion for the open circuit back emf is also kept as low as 1.103%. All design goals were reached successfully.

For practical applications, future work should be focused on transient analysis. For system stability and reliability, great attention also needs to be paid to structural design. Mechanical drawings for the final structural design will be submitted for the manufactory of the motor. After the motor being built, the whole PMSM drive will be constructed with the existing inverter and bearing system. Future studies and analysis will be carried out on the whole PMSM system to obtain realistic data for the practical application.

Bibliography

[1] V. Sreedhar, “Plug-In Hybrid Electric Vehicles with Full Performance” IEEE Conference on Electric and Hybrid Vehicles, ICEHV 2006, December, 2006, Page(s):1 – 2.

[2] K. Nishibata, M. Ishida, S. Doki, T. Masuzawa, M. Fujitsuna, “Speed Estimation Method utilizing Rotor Slot Harmonics Detected from Line Current for Speed Sensorless Drive of Ultra High Speed Induction Machine” IEEE Transactions on Industrial Technology, 2006, Page(s):1591-1596.

[3] J. Wang, F. Wang, and X. Kong, “Design and analysis of electromagnetic properties of high speed PM generator” Proceeding of CSEE 2008, vol. 28, 2008, Page(s):105–109.

[4] A. Emadi, “Handbook of Automotive Power Electronics and Motor Drives” CRC Press Taylor & Francis Group, 2005.

[5] J. Beno, R. Thompson, R. Hebner, “Flywheel batteries for vehicles” Proceedings of the 2002 Workshop, Autonomous Underwater Vehicles, June, 2002, Page(s):99-101.

[6] R. E. Horner, N. J. Proud, “The key factors in the design and construction of advanced flywheel energy storage systems and their application to improve telecommunication power back-up” IEEE Transactions on Telecommunications Energy Conference, 1996, Page(s):668-675.

[7] R. C. Wagner, D. R. Boyle, K. Decker, “Commercialization of flywheel energy storage technology on the international space station” IEEE Conference on Energy Conversion Engineering Conference, IECEC 2002, 2002, Page(s):146-150.

[8] P. P. Acarnley, B. C. Mecrow, J. S. Burdess, J. N. Fawcett, J. G. Kelly, P. G. Dickinson, “Design principles for a flywheel energy store for road vehicles ” IEEE Transactions on Industry Applications Conference, Thirtieth IAS Annual Meeting, 1995, Page(s):672-678.

[9] J. Zhang, Z. Chen, L. Cai, Y. Zhao, “Flywheel energy storage system design for distribution network” IEEE Conference on Power Engineering Society Winter Meeting, Vol. 4, 2000, Page(s):2619-2623.

[10] D. H. Curtiss, P. P. Mongeau, R. L. Puterbaugh, “Advanced composite flywheel structural design for a pulsed disk alternator” IEEE Transactions on Magnetics, Vol. 31, Issue 1, Part 1, 1995, Page(s):26-31.

[11] K. W. Lee, J. Yi, B. Kim, J. Ko, “Micro generator using flywheel energy storage system with high-temperature superconductor bearing” IEEE 20th International Conference, Micro Electro Mechanical System, 2007, Page(s):875-878.

[12] R. C. Dorf, “The Engineering Handbook Second Edition” CRC Press LLC, 2005.

[13] M. Ehsani, Y. Gao, S. E. Gay, A. Emadi, “Modern Electric Hybrid Electric and Fuel Cell Vehicles Fundamentals Theory and Design” CRC Press LLC, 2005.

[14] S. A. Nasar, I. Boldea, “Electric Machines Steady-State Operation” Hemisphere Publishing Corporation, 1990.

[15] S. H. Han, T. M. Jahns, Z. Q. Zhu, “Analysis of Rotor Core Eddy-Current Losses in Interior Permanent Magnet Synchronous Machines” Industry Applications Society Annual Meeting, October, 2008, Page(s):1 – 8.

[16] P. J. Hor, Z. Q. Zhu, D. Howe, J. Rees-Jones, “Eddy-current loss in a moving-coil linear tubular permanent magnet brushless motor” IEEE Transactions on Magnetics, vol.35, no.5, 1999, Page(s):3601–3603.

[17] Y. Yu, F. Chai, S. Cheng, “Analysis of modulation pattern and losses in inverter for PMSM drives” IEEE Conference on Vehicle Power and Propulsion, VPPC 08, September, 2008, Page(s):1 – 4.

[18] A. M. EL-Refaie, T. M. Jahns, “Comparison of synchronous PM machine types for wide constant-power speed operation: converter performance” IET Electric Power Applications, vol. 1, March 2007, Page(s):217–222.

[19] M. Jiang, J. Salmon, A. M. Knight, “Design of a permanent magnet synchronous machine for a flywheel energy storage system within a hybrid electric vehicle” IEEE Conference on Electric Machines and Drives Conference, IEMDC 2009, May 2009, Page(s):1736 – 1742.

[20] N. Schofield, K. Ng, Z. Q. Zhu, D. Howe, “Parasitic rotor losses in a brushless permanent magnet traction machine” Eighth International Conference on Electrical Machines and Drives, September 1997, Page(s):200 – 204.

[21] L. Zheng, T. X. Wu, D. Acharya, K. B. Sundaram, J. Vaidya, L. Zhao, “Design of a super-high speed permanent magnet synchronous motor for cryogenic applications” IEEE International Conference on Electric Machines and Drives, May 2005, Page(s):874 – 881.

[22] C. C. Mi, G. R. Slemon, R. Bonert, “Minimization of iron losses of permanent magnet synchronous machines” IEEE Transactions on Energy Conversion, vol. 20, Issue 1, March 2005, Page(s):121 – 127.

[23] F. Deng, “An improved iron loss estimation for permanent magnet brushless machines” IEEE Transaction on Energy Conversion, vol.14, no.4, December 1999, Page(s):1391–1395.

[24] D. C. Hanselman, “Brushless permanent-magnet motor design” McGraw-Hill, 1994.

[25] N. Boules, “Impact of slot harmonics on losses of high-speed permanent magnet machines with a magnet retaining ring” Proceedings on Electric Power Components and Systems, vol. 6, no. 6, November 1981, Page(s):527-539.

[26] K. Atallah, D. Howe, P. H. Mellor, D. A. Stone, “Rotor loss in permanent magnet brushless ac machines” IEEE Transaction on Industry Applications, vol. 36, no. 6, 2000, Page(s):1612-1618.

[27] S. J. Salon, “Finite Element Analysis of Electrical Machines” Norwell, MA: Kluwer Academic Publishers, 1995.

[28] J. V-D. Veen, L. Offringa, A. Vandenput, “Minimixing Rotor Losses in High-Speed High-Power Permanent-magnet Synchronous Generator with Rectifier Load” IEEE Proceedings of Electrical Power Applications, Vol. 144, No. 5, September 1997, Page(s):331-337.

[29] J. Kobuchi, K. Oobayashi, R. Shimada, “Windage loss reduction of flywheel/generator system using He and SF 6 gas mixtures” IEEE Transactions on Energy Conversion Engineering Conference, IECEC 97, Volume 3, July 27th-Aug 1st. 1997, Page(s):1754 – 1757.

[30] R. L. Nailen, “Stray Load Loss: What’s it all about?” Electrical Apparatus, Aug., 2007.

[31] N. Urasaki, T. Senjyu, K. Uezato, “An accurate modeling for permanent magnet synchronous motor drives” IEEE Transactions on Applied Power Electronics Conference and Exposition, Fifteenth Annual APEC 2000, Volume 1, February 2000, Page(s):387 – 392.

[32] Y. Zhan, “Stray Loss Analysis of AC Machines Using Time-stepped Finite Elements” Thesis for Doctor of Philosophy In Field of Power Engineering and Power Electronics, University Of Alberta, 2010.

[33] T. D. Batzel, K. Y. Lee, “Slotless Permanent Magnet Synchronous Motor Operation without a High Resolution Rotor Angle Sensor” IEEE Transactions on Energy Conversion, Vol. 15, No. 4, December 2000, Page(s): 366-371.

[34] G. Zhang, F. Wang, Y. Shen, “Reduction of rotor loss and cogging torque of high speed PM machine by stator teeth notching” International Conference on Electrical Machines and Systems, ICEMS 2007, October 2007 Page(s):856 – 859.

[35] F. Aschenbrenner, “Innovation on Traditional Water Wheels for Renewable Energy” IEEE Conference on Power Electronics and Motion Control, EPEPEMC 2006, 2006, Page(s):1625-1630.

[36] F. Aschenbrenner, H. Weiss, “Low Speed Rare Earth Permanent Magnet Synchronous Generator for Gearless Coupling to Water Wheel” International Conference on Electrical Drives and Power Electronics, EDPE 2007, September 2007.

[37] W. Czernin, H. Weiss, F. Aschenbrenner, “Low cost cogging torque elimination at PMSM by power electronics control” 9th International Conference on Electronic Instrument Engineering, APEIE 2008, vol. 01, September 2008, Page(s):145 – 150.

[38] K. Gulez, A. A. Adam, H. Pastaci, “Torque Ripple and EMI Noise Minimization in PMSM Using Active Filter Topology and Field-Oriented Control” IEEE Transactions on Industrial Electronics, vol. 55, no. 1, January 2008, Page(s):251 – 257.

[39] H. Fujita, T. Yamasaki, H. Akagi, “A hybrid active filter for damping of harmonic resonance in industrial power systems” IEEE Transactions on Power Electronics, vol. 15, no. 2, March 2000, Page(s):215–222.

[40] P. Degober, G. Remy, J. Zeng, P. J. Barre, J. P. Hautier, “High performance control of the permanent magnet synchronous motor using self-tuning resonant controllers” Proceeding of the 38th Southeastern Symposium on System Theory, March 2006, Page(s):382–386.

[41] N. Bianchi, S. Bolognani, F. Luise, “Analysis and design of a PM brushless motor for high-speed operations,” IEEE Transactions on Energy Conversion, vol.20, no.3, September 2005, Page(s):629-637.

[42] A. S. Nagorny, N. V. Dravid, R. H. Jansen, B. H. Kenny, “Design aspects of a high speed permanent magnet synchronous motor / generator for flywheel applications” IEEE International Conference on Electric Machines and Drives, May 2005, Page(s):635 – 641.

[43] D. Gerada, A. Mebarki, C. Gerada, “Optimal design of a high speed concentrated wound PMSM” IEEE International Conference on Electrical Machines and Systems, ICEMS 2009, Page(s):1-6.

[44] P. C. Krause, O. Wasynczuk, S. D. Sudhoff, “Analysis of electric machinery and drive systems, second edition” Wiley-IEEE Press, 2002.

[45] I. Takahashi, T. Noguchi, “A New Quick Response and High-Efficiency Control Strategy of an Induction Motor” IEEE Transactions on Industry Applications, September 1986, vol. 1, Page(s):820–827.

[46] T. G. Habetler, F. Profumo, M. Pastorelli, L. M. Tolbert, “Direct torque control of induction machines using space vector modulation” IEEE Transactions on Industry Applications, vol. 28, Issue 5, September 1992 Page(s):1045 – 1053.

[47] D. Rachid, H. Othman, B. Faouzi, “A completely vectored direct torque control scheme for induction motor” IEEE International Conference on Systems, Man and Cybernetics, SMC 2002, vol. 5, October 2002, Page(s):6.

[48] R. K. Sharma, V. Sanadhya, L. Behera, S. Bhattacharya, “Vector control of a permanent magnet synchronous motor” Annual IEEE India Conference, INDICON 2008, vol. 1, December 2008, Page(s):81 – 86.

[49] L. Zhong, M. F. Rahman, W. Y. Hu, K. W. Lim, M. A. Rahman, “A Direct Torque Control For Permanent Magnet Synchronous Motor Drives” IEEE Transactions on Energy Conversion, Vol. 14, No. 3, September 1999

[50] T. H. Liu, C. H. Liu, “A multiprocessor-based fully digital control architecture for permanent magnet synchronous motor drives” IEEE Transactions on Power Electronics, vol. 5, no. 4, October 1990, Page(s):413-423.

[51] J. F. Gieras, “Permanent Magnet Motor Technology Design and Applications, third Edition” CRC Press, 2010.

[52] N. Bianchi, S. Bolognani, F. Luise, “Analysis and Design of a PM Brushless Motor for High-Speed Operations” IEEE Transactions on Energy Conversion, Vol. 20, Issue 3, 2005, Page(s):629-637.

[53] R. Krishnan, “Permanent Magnet Synchronous and Brushless DC Motor Drives” CRC Press Taylor & Francis Group, 2010.

[54] K. Yamazaki, “Loss Analysis of Permanent Magnet Motors with Concentrated Windings-Variation of Magnet Eddy Current Loss Due to Stator and Rotor Shapes” IEEE Conference on Industry Applications Society Annual Meeting, IAS 08, September 2008, Page(s):1-8.

[55] Q. Liu, M. A. Khambadkone, “Design Optimization of Wide-speed Permanent Magnet Synchronous Motors” IEEE Conference on Power Electronics, Machines and Drives, no. 487, June 2002, Page(s):404-408.

[56] C. A. Gross, “Electric Machines” CRC Press, Taylor & Francis Group, 2007.

[57] M. Sanada, S. Morimoto, “Efficiency Improvement in High Speed Operation using Slot-less Configuration for Permanent Magnet Synchronous Motor” IEEE Power Engineering Society General Meeting, June 2007 Page(s):1 – 7.

[58] H. A. Toliyat, G. B. Kliman, “Handbook of Electric Motors, Second Edition, Revised and Expanded” CRC Press, Taylor & Francis Group, 2004.

[59] S. J. Chapman, “Electric Machinery Fundamentals, Third Edition” McGraw-Hill Companies, Inc., 1999.

[60] R. Krishnan, “Control and operation of PM synchronous motor drives in the field-weakening region” Proceedings of Industrial Electronics, Control, and Instrumentation, IECON 1993, vol. 2, November 1993, Page(s):745 – 750.

[61] J. Chen, K. Chin, “Minimum copper loss flux-weakening control of surface mounted permanent magnet synchronous motors” IEEE Transactions on Power Electronics, vol. 18, Issue 4, July 2003, Page(s):929 – 936.

[62] Z. Q. Zhu, Y. S. Chen, D. Howe, “Maximizing the flux-weakening capability of permanent magnet brushless AC machines and drives” Proceedings of Power Electronics and Motion Control Conference, IPEMC 2000, vol. 2, August 2000, Page(s):552 – 557.

Appendix A-1

Mechanical Drawing for the Stator Structure

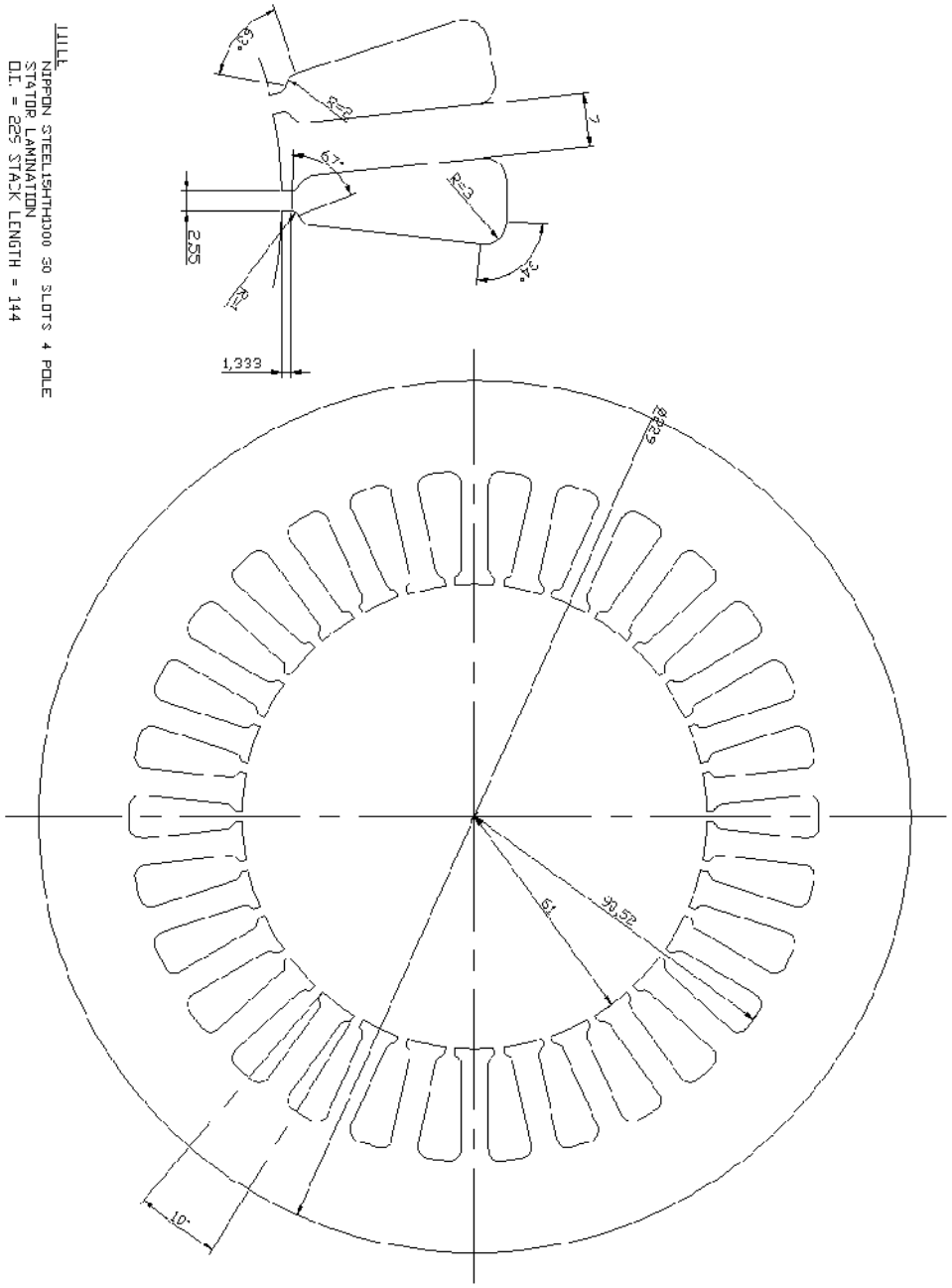

Appendix A-2

Mechanical Drawing for the Rotor Structure

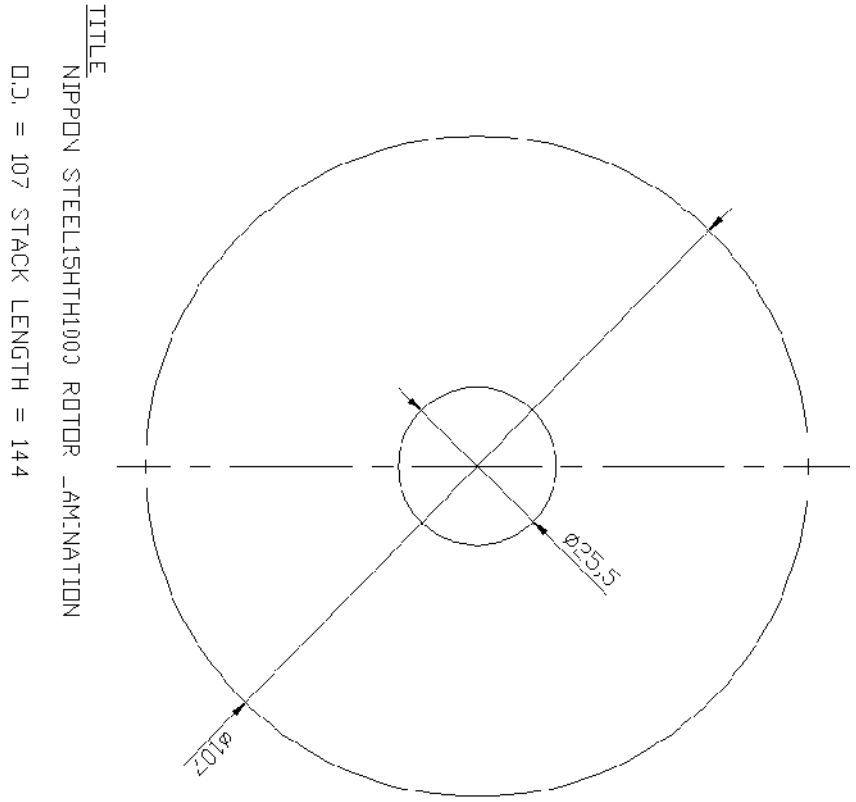

Appendix A-3

Mechanical Drawing for the Magnet Structures